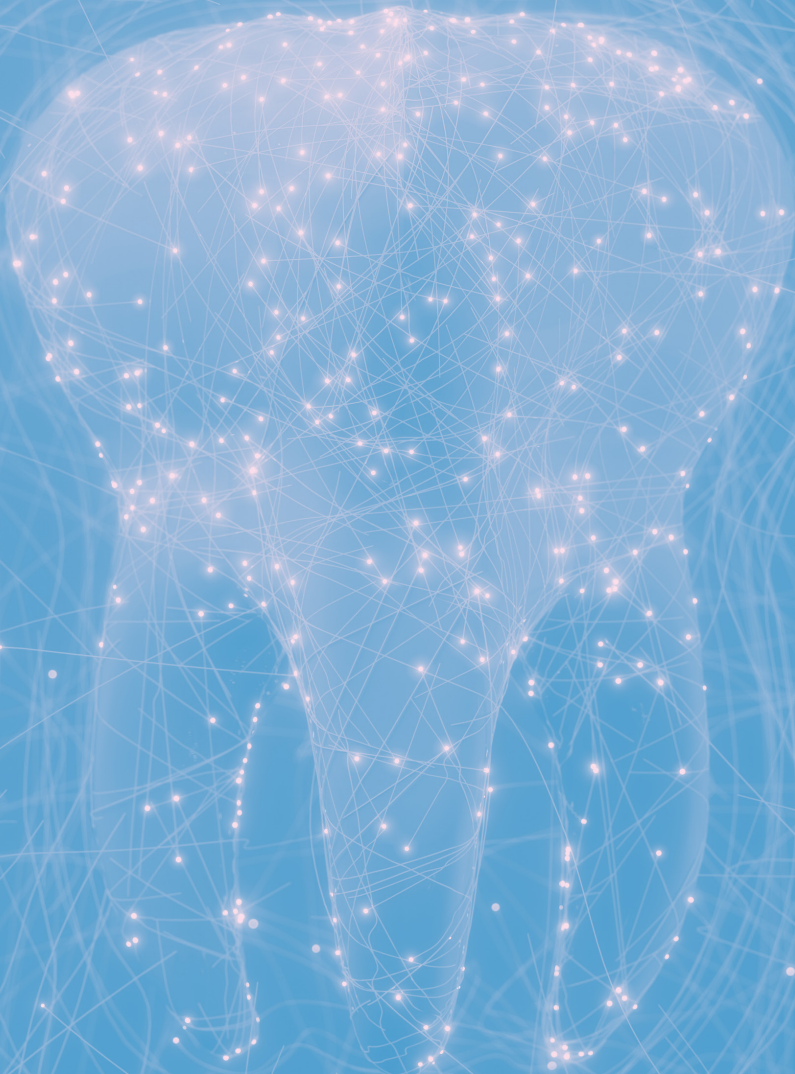# Research Day
2024

Thursday, March 7

Robertson Life Science Building, Portland, OR

OHSU

SCHOOL OF DENTISTRY

Research Day
2024

Thursday, March 7

Robertson Life Science Building, Portland, OR

OHSU

Thursday, March 7, 2024

8:00 am   Poster setup
RLSB Atrium
Refreshments such as coffee, tea, pastries, fruit, and bagels will be provided.

8:30 am   Poster Session #1
(odd numbers)

10:10 am Poster Session #2
(even numbers)

12 noon   Keynote
In-person
RLSB 3A003A/B
online via Webex

Sack lunches will be offered on a first-come, first-served basis for attendees remaining for the lecture.

A special thank you to

Drs. Barry Taylor and Mark Mutschler
OREGON DENTAL ASSOCIATION

Drs. Cyrus Lee and Dan Philstrom
PERMANENTE DENTAL ASSOCIATES

Dr. Lisa Bozzettii
VIRGINIA GARCIA MEMORIAL HEALTH CENTER

Research Day Special Guest Speakers

David Huang, MD, PhD

Seeing Small and Aiming Big: the Development and Clinical Impact of Optical Coherence Tomography

Alireza Sadr, DDS, PhD

Dental Optical Coherence Tomography: Benchside to Chairside

Research Day
2024

Poster Session #1 (*Odds*)

8:30-10:00am

Thursday, March 7

Robertson Life Science Building, Portland, OR

OHSU

Research Day

Poster Session #1 (Odds) – Posters and Abstracts Alphabetical by Presenter's last name
Note: CaseCATs do not have associated Abstracts.

Name	Poster Number	Category	Title
Islam Ali	21	POSTDOC	Enteroccocus faecalis attenuates Parvimonas micra biofilms via a pH-dependent effect
David Anderson	11	STAFF	Click-FAST: A Customizable Anaerobic Fluorescence Platform for Live-cell Imaging
Avathamsa Athirasala	39	POSTDOC	Nuclear Deformation and Rupture during Intravascular Migration through a Mineralized Matrix are Key Mediators of Prostate Cancer Metastasis to Bone
Philopater Badawi	47	CaseCAT	The Performance of Photon-Counting X-Ray Sensors when Imaging Hard Tissues for Dental Applications
Joao Batista	15	PhD STUDENT	Functionalization of Urea-Melamine-Formaldehyde Microcapsules for Self-healing Dental resin application
Lauren Chao	23	RESIDENT	A retrospective study evaluating moderate sedation success pre-COVID-19 and in the COVID-19 era
May Anny Fraga	35	PhD STUDENT	Osteoclast-Independent Bone Invasion in Head and Neck Squamous Cell Carcinoma: A 'Bone-on-a-Chip' Model Study.
Tapas Ghosh	19	POSTDOC	Injectable, Robust, Biocompatible Hydroxyapatite Nanoparticle Embedded Chitosan-Based Hydrogel with Potent Antibacterial Activity
Emily Helliwell	37	STAFF	Immunostimulatory effects of Extracellular Membrane Vesicles From Oral Commensal Streptococcus sanguinis
Hung, Angela	53	CaseCAT	Direct Pulp Capping on Permanent Teeth with Carious Pulp Exposure
Bao Huynh	27	STAFF	An Enzyme-Responsive Nanoplatform for Preventing Collagen Degradation in Dental Tissues
Laura Iwasaki (MS Thesis of Angela Li)	5	FACULTY	The short-term effects of orthognathic surgery on condylar orientation and positions in bilateral sagittal split osteotomy patients
Matt Jervis	25	RESIDENT	Assessing obturation voids between radicular dentin and single cone gutta percha using CBCT in root canal prepared teeth.
Hayden Lackey**	43	STUDENT	Variable Polydispersity among beta-Crystallin Homodimers via Dynamic Light Scattering
Luke Miller	29	STAFF	Functionalization of glass surfaces for anti-biofilm properties for dental restorative materials
Stephanie Momeni	17	FACULTY	The critical significance of Streptococcus mutans studies beyond UA159
Jeff Nickel	7	FACULTY	Autonomic Function and Muscle Activity in Growing Children
Jonathan Nguyen	51	CaseCAT	Treatment Efficacy of Conservative and Radical management on Ameloblastoma
Branden Pelzer and Emily Tran	55	CaseCAT	Efficacy of Stannous Fluoride Toothpaste as a Remedy for Patients with Dentinal Hypersensitivity
Hua Qin	33	STAFF	Development of a versatile toolbox for genetic manipulation of Prevotella melaninogenica
Sivashankari Rajasekaran	13	POSTDOC	Reinforcing Urea-Formaldehyde Microcapsules Stability through Additive Modulation
Nidhi Satasia and Katherine Ouda	57	CaseCAT	Treatment for Cracked Tooth Syndrome
Jill Sukraw	49	CaseCAT	Efficacy of Treating Severe Deep Bite with Clear Aligner Therapy
Jonah Tang	1	STAFF	Unsaturated fatty acids impact the physiology and virulence of Streptococci
Fernanda Tsuzuki	31	PhD STUDENT	Tailoring material surface chemistry to control acquired pellicle composition
Erin Waid	45	RESIDENT	Assessing obturation voids between radicular dentin and single cone gutta percha using a novel photon counting intraoral sensor
Samuel Weber	9	STAFF	Use of Dental Adhesives to Improve Bond Strength of Titanium Implants to Bone
Zhengzhong Zou	41	STAFF	Visualizing and monitoring pH in Veillonella and Streptococci biofilms using HaloTag

OHSU

Enterococcus faecalis attenuates Parvimonas micra biofilms via a pH-dependent effect

Islam Ali
PostDoctoral Scholar, Wu lab, OHSU School of Dentistry

Introduction
Parviomonas micra and Enterococcus faecalis are two frequently isolated microorganisms from secondary/persistent apical periodontitis, a polymicrobial-biofilm mediated disease of dental root canal system and surrounding periapical tissues. Their coexistence implies a potential interspecies interaction which remains unexplored. The main objective of this study was to determine the effect of E. faecalis cell-free supernatants on P. micra biofilms.

Methods
E. faecalis was allowed to grow under anerobic conditions for 1, 6 or 24 hours, at which the cell-free supernatants were obtained. Pre-formed P. micra biofilms (24h-old) under anerobic atmosphere on tissue culture-treated microplates were further incubated with or without E. faecalis supernatants for 24 hours. In another experiments, P. micra biofilms were treated with heat-inactivated or pH-neutralized 6-h supernatants. P. micra biofilm without E. faecalis supernatants served as control in all experiments. Biomass and viability of P. micra biofilms were evaluated using crystal violet and colony forming units (CFUs) assays, respectively. Fluorescent labelling with SYTO 9/TOTO-3 was performed to visualize P. micra biofilms developed under E. faecalis neutralized and non-neutralized supernatants. Statistical analysis was performed using the parametric ANOVA and post-hoc Tukey's or the non-parametric Kruskal-Wallis and post-hoc Dunn tests ($P = 0.05$).

Results
E. faecalis 6- and 24-h supernatants significantly decreased the biomass and viability of P. micra biofilms ($P < 0.05$) irrespective of the supernatant concentration. P. micra biofilms developed in the presence or absence of heat-inactivated supernatants were not significantly different ($P > 0.05$). P. micra biofilms developed under neutralized supernatants had significantly higher biomass and viable cell counts compared to those under non-neutralized supernatants ($P < 0.05$) without being significantly different from control biofilms. The structure of P. micra biofilm was attenuated by E. faecalis supernatant and partially restored when exposed to a pH-neutralized supernatant.

Conclusions
The effect of E. faecalis on P. micra biofilms is not mediated via heat-labile protein(s). E. faecalis attenuates P. micra biofilms by generating an acidic environment.

Click-FAST: A Customizable Anaerobic Fluorescence Platform for Live-cell Imaging

David Anderson
Senior Research Associate, Merritt lab, OHSU School of Dentistry

Co-Authors: Matthew G. Logan, Sarah S. Patty, Alexander J. Kendall†, Christina Z. Borland, Carmem S. Pfeifer, Jens Kreth, and Justin L. Merritt

†Current Address: Pacific Northwest National Laboratory, Richland, WA, USA

Introduction

Humans harbor as many bacterial cells as those composing our own bodies. The majority of them reside in hypoxic environments, and many of our most vexing bacterial pathogens are strict anaerobes. The recently developed fluorescence-activating and absorption-shifting tag (FAST) protein-fluorogen system is a promising technology for use in live-cell fluorescence imaging within an anaerobic atmosphere. This work seeks to construct a platform which combines azide-alkyne cycloaddition (click chemistry) with a robust and affordable fluorogen for mechanistic studies. This simple approach will result in easily modifiable reagents to query physiological parameters such as: differential permeability, transport, and enzymatic activity.

Methods

Two alkyne-linked fluorogens were synthesized for downstream click reactions. One fluorogen, referred to as Poppy, was based on previous literature and it emits at a far-red wavelength. A second novel fluorogen incorporating ethyl vanillin, a cheap and abundant flavoring agent, is introduced here. The molecule is referred to as Blaze and it exhibits highest emission at a yellow-orange wavelength. Functionalized derivatives were directly added to cultures of Streptococcus mutans UA159 and/or Escherichia coli BL21 expressing a tandem-linked dimer of the fluorescence-activating and absorption-shifting tag (FAST) protein. A control strain of Escherichia coli harboring a plasmid expressing monomeric FAST as an outer membrane fusion protein was also used. Imaging was conducted using a wide-field fluorescence microscope equipped with an atmospheric chamber which was typically set produce a 0.1% oxygen and 5% carbon dioxide environment. All images for each indicated experimental set where acquired and processed in identical fashion using a combination of Olympus and Fiji software. In vitro experiments were conducted using recombinantly-purified FAST proteins, and data was acquired on a Cytation5 multimodal plate reader. Data isotherms were then fit via non-linear regression (single site binding mode) using Prism 9.5.1.

Results

We found that the FAST system is robustly fluorescent in hypoxic environments. Significant signal remained after minutes of photon exposure. Increasing oxygen, from 0.1 to one, five or ambient oxygen levels lead to concomitant increased bleaching rates. Click reactions linking two different alkyne fluorogen variants to several azide linked molecules showed that fluor binding and fluorescence emission is likely to be preserved over an array of possible click partners. We found that fluorogens conjugated to azido-benzoic acid were able to penetrate into Streptococcus mutans, but not Escherichia coli. Lactose-conjugated molecules were poorly able to enter either species, but a small subset of E. coli did emit fluorescence. A large PEGylated-conjugate was tested and it exhibited stringently non-permeable characteristics compared to the gold standard propridium iodide (PI). We titrate chlorhexidine against E. coli to show that sub lethal disruption of the membrane barrier presents more PI signal compared to PEG-FAST.

Conclusions

Click-FAST will be an asset for fluorescence microscopists requiring hypoxic conditions. Removal of oxygen greatly enhances the emission stability, which will bode well for low signal scenarios. We introduce a cheap alternative to commercially-available fluorogens in this work to alleviate expense bottlenecks. The clickable nature of this reagent lends itself to be useful to nearly any laboratory wishing to functionalize their fluorophores. We show several conjugants retain fluorescence activity and display some useful properties in two model organisms. Click-FAST may be a promising tool to dissect biological phenomena or to discover new chemicals if combined with large click-compatible chemical libraries.

Nuclear Deformation and Rupture during Intravascular Migration through a Mineralized Matrix are Key Mediators of Prostate Cancer Metastasis to Bone

Avathamsa Athirasala

PostDoctoral Scholar (T90 PORT Trainee), Bertassoni lab, OHSU School of Dentistry

Co-Authors: Avathamsa Athirasala1,2,3, Cristiane M. Franca1,2,3, Amin Mansoorifar1,3, Ramesh Subbiah1,3, Maria E. Q. Lima Verde3, May Anne Fraga1,2,3, Doug Keene7, Luiz Bertassoni1,2,3,4,5,61 Knight Cancer Precision Biofabrication Hub, Knight Cancer Institute, Oregon Health and Science University
2 Cancer Early Detection Advanced Research Center (CEDAR), Knight Cancer Institute, OHSU
3 Division of Biomaterials and Integrative Biosciences, School of Dentistry, OHSU
4 Division of Oncological Sciences, School of Medicine, OSHU
5 Department of Biomedical Engineering, School of Medicine, OHSU
6 Center for Regenerative Medicine, OHSU
7 Microimaging Center, Shriner's Hospital for Children

Introduction
Several neoplastic diseases preferentially target bone tissue, which presents a substantially different microenvironment from that of the primary tumor. Both the physical properties of the bone microenvironment as well as the biological function of its diverse population of resident cells are derived from the unique nanoscale structure and chemical composition of its highly calcified matrix, which is likely to also play a significant role in the survival and growth of metastatic tumor cells. However, these key interactions are far from being understood, given that current in-vitro bone models fail to replicate the structural, cellular and extracellular complexity of native bone. Here, we developed and characterized a novel bone-on-a-chip platform that replicates the critical hallmarks of bone tissue.

Methods
The platform constitutes a microfluidic model of nanoscale mineralized cell-laden collagen hydrogel, incorporating embedded osteoblasts, osteocytes, mesenchymal stem cells and a perfusable pericyte-supported vasculature interacting with circulating prostate cancer cells.

Results
The on-chip format of the platform enables live tracking of early metastatic events such as transendothelial migration and extravasation, where prostate cancer cells were observed to have a clear predilection for dissemination through the engineered microvasculature into the bone like matrix when compared to non-mineralized scaffolds. Moreover, it was evident that the process of intravascular migration and extravasation through the more constrictive and calcified matrix induced significant nuclear deformation, rupture and DNA damage pointing to possible mechanisms through which the bone microenvironment could contribute to genomic instability and acquisition of more aggressive phenotypes following metastasis.

Conclusions
In conclusion, the engineered bone on a chip platform elucidated novel mechanisms driving metastatic cancer progression in bone tissues.

Functionalization of Urea-Melamine-Formaldehyde Microcapsules for Self-healing Dental resin application

Joao Batista

PhD Student, Fugolin lab, OHSU School of Dentistry

Co-Authors: Bao Huynh, Sivashankari Rajasekaran, Mario Sinhoreti (Department of Restorative Dentistry / State University of Campinas), Ana Paula Fugolin

Introduction
Self-healing composites are developed to prevent catastrophic failures in restored teeth under thermal and masticatory stresses. This technology involves encapsulating a healing agent inside stimuli-responsive microcapsules, which rupture upon the occurrence of microcracks in the material structure. A limitation of this strategy is the lack of chemical bonding between the microcapsule shells and the organic matrix, which poses a challenge for the microcapsule rupture and restricts the amount that can be incorporated without compromising mechanical properties. Therefore, this study aims to design, synthesize, and characterize poly(urea-melamine-formaldehyde) (PUMF)-functionalized microcapsules as a strategy to enhance the performance of self-healing restorative dental materials.

Methods
PUMF microcapsules were synthesized by double emulsion method using mechanical stirring. The urea-formaldehyde shell was modified with 5% melamine, encapsulating the healing agent formed by 80% of triethylene glycol dimethacrylate (TEGDMA) + 20% of dimethylaminoethyl methacrylate (DMAM). N,N-Bis(2-hydroxyethyl)-p-toluidine (DHEPT) was used as a chemical co-initiator incorporated to the healing agent. Poly(urea-formaldehyde) (PUF) were used as a negative control. Microcapsules surfaces were functionalized with 4% triethoxysilane (TeOs), 4% (3-Aminopropyl)triethoxysilane (APTES), or (3-mercaptopropyl)trimethoxysilane (MPTMS). Considering different protocols, the seven tested experimental groups were PUMF, PUF, TeOS, APTES, MPTMS, TeOs + APTES, TeOs + MPTMS. Morphological characterization was observed by optical and scanning electron (SEM) microscopies. Thermogravimetric analysis (TGA) was performed for all the groups. The microcapsules were then added at 10 wt% into a dental resin formulation composed of bisphenol A-glycidyl methacrylate (BisGMA), ethoxylated bisphenol-A dimethacrylate (BisEMA), urethane dimethacrylate (UDMA), and TEGDMA at a 2:2:2:1 weight ratio. Benzoyl peroxide (BPO) and phenylbis (2,4,6-trimethylbenzoyl)phosphine oxide (BAPO) were added at 0.5 wt% and 1.0 wt%, respectively. V-notch fracture toughness bars were prepared (n=6), fractured catastrophically (F1), left to heal for 24 hours, and then re-subjected to the test (F2). Healing percentage (%) of the bars were calculated by the formula: F2/F1 x 100. Photos of the bars were taken immediately after the catastrophic fracture and after healing for 24 hours using a DSLR camera. SEM of the bars fractured area were performed. The data was statistically analyzed by two-way ANOVA and Tukey's test.

Results
TGA data have confirmed the successful modification of the shells, as there is a noticeable change in the curve profile and a pronounced shift to the right. Additionally, the remaining mass increased for the functionalized microcapsules, likely related to the formation of silicon groups. The preservation of the integrity of the microcapsule shells and their cargoes was confirmed by optical and scanning electron microscopies. Regarding healing efficiency, the results ranged from 0 to 35±9.3%, with the lowest results shown by PUF and the highest for TEOS + MPTMS. This may be attributed to a synergistic effect between shell reinforcement and brittleness

resulting from the silica coating (TEOS) and the optimized rupture of the microcapsules induced by the chain-transfer reactions performed by the pendant thiol groups (MPTMS).

Conclusions
Overall, PUMF-functionalized microcapsules were synthesized and characterized. Their incorporation into dental resin formulations resulted in a substantial increase in the healing performance of the systems. The next steps will involve validating the microcapsule-containing formulations in clinically mimicked scenarios and investigating the microstructural changes induced by the chemical bonding between the shells and the organic matrix regarding microcrack formation and propagation.

A retrospective study evaluating moderate sedation success pre-COVID-19 and in the COVID-19 era.

Lauren Chao
Resident, Pediatric Dentistry, OHSU School of Dentistry

Co-Authors: Dongseok Choi PhD

Introduction

Dental caries is known as the most common chronic childhood infectious disease, which untreated can lead to significant decreased quality of life. One way to safely and reliably treat dental caries is under general anesthesia. Since the outbreak of the COVID-19 pandemic, access to hospitals and general anesthesia has decreased and waitlists have increased. Moderate sedation is being used in our clinic more frequently in an attempt to manage dental disease. The goal of this study is to evaluate these moderate sedation appointments and compare the success rates in the years prior to the COVID-19 outbreak and since COVID-19 outbreak.

Methods

Approval from OHSU IRB was obtained (#25572). A retrospective chart review of all patients who had CDT code D9248 "Non-IV conscious sedation" completed between January 2017 and October 4, 2023, was done and separated into two groups: those who had treatment done pre-COVID outbreak and restrictions and those who had treatment in the era of COVID-19. The following information was gathered: age of patient in years at the time of treatment, number of moderate sedation appointments, number of sextants treatment planned, whether general anesthesia was recommended but moderate sedation was attempted, whether all intended treatment was completed under moderate sedation, whether a change in treatment modality was recommended and whether that change was due to cooperation of the patient or appropriateness of treatment. Patients who were lost to follow up, did not complete treatment, or in active treatment at the time of data collection were excluded from analysis. Information was analyzed with descriptive statistics. Differences between pre- and in COVID-19 were assessed by t-test and chi-square test. A P-value of 0.05 was used to determine significance.

Results

There were 193 patients included pre-COVID-19 and 175 patients included during the COVID-19 era. Between those patients seen pre-COVID-19 and during the COVID-19 era, there were no statistical differences in the ages of pediatric patients undergoing dental treatment under moderate sedation, the number of moderate sedation appointments for each patient seen, the number of sextants requiring treatment in patients receiving moderate sedation, whether a change in treatment modality was recommended, or whether the change in modality was due to patient cooperation or appropriateness of treatment needs. Modality changes include: general anesthesia, traditional restorative treatment with or without nitrous oxide, or minimally invasive dentistry techniques. General anesthesia was recommended but treatment under moderate sedation was attempted significantly more often for pediatric patients in the COVID-19 era than pre-COVID-19, and there was a statistically significant difference in whether or not all recommended dental treatment was completed under moderate sedation.

Conclusions

There has been a significant decrease in cases successfully completed under moderate sedation since the outbreak of COVID-19. While moderate sedation can be an effective

advanced behavior guidance technique, it does not replace general anesthesia as a treatment modality. Appropriate access to general anesthesia for pediatric dental providers is still necessary to safely and effectively treat our pediatric dental population.

Osteoclast-Independent Bone Invasion in Head and Neck Squamous Cell Carcinoma: A 'Bone-on-a-Chip' Model Study.

May Anny Fraga
PhD Student, Bertassoni lab, OHSU School of Dentistry

Co-Authors: Cristiane Miranda Franca, Mauricio Sousa, Avathamsa Athirasala, Sofia Vignolo, Americo Correr*, Luiz Bertassoni.
* Restorative Dentistry, Piracicaba Dental School - UNICAMP

Introduction

Head and neck squamous cell carcinomas (HNSCC) present a challenge due to their tendency to invade nearby bones. Originating from mucosal epithelial cells in regions like the oral cavity, pharynx, larynx, and sinonasal tract, these cancers exhibit bone invasion in over 50% of patients at diagnosis, categorizing them as advanced primary tumors (T4). This classification is associated with poor overall survival and high local recurrence rates. Current treatments involve aggressive approaches, including surgical removal of affected bone, radiotherapy, and chemotherapy, resulting in functional and aesthetic deficits. However, the early mechanisms of HNSCC bone invasion are not fully understood, often making a conservative approach impractical upon detection. Morphologically, bone invasion in HNSCC is described as erosive or infiltrative. The erosive pattern, typically osteoclast-dependent, has minimal impact on survival, while the infiltrative pattern, marked by tumoral cells in deep cortical bone marrow (mostly osteoclast-independent), negatively affects prognosis. The sequence of HNSCC cell aggressiveness and bone invasion, and the role of specific signals from bone cells and the extracellular matrix (ECM), remain unclear. Our overarching goal is to understand the role of the bone mineralization and osteoblast/osteocytes on the invasive behavior of HNSCC.

Methods

To understand the osteoclast-independent invasion mechanism, we utilized a "bone-on-a-chip" model composed of microfluidic device with a central chamber separated from two parallel channels by pillars. The chamber was filled with matrix of a mixture of collagen (2.5 mg/mL-1), fibrin, and thrombin, with or without osteoblasts ($3x10^6$ cells/mL). The matrix was then mineralized for three days in a solution of $CaCl_2.2H_2O$, osteopontin, and K_2HPO_4. The mineralization process induced osteoblast differentiation in osteocytes. Subsequently, oral squamous cell carcinoma (OSCC) cells were seeded into a lateral channel and cultured for 3 days.

Results

OSCC interacted with the ECM with and without osteoblast, showing migration, and morphological changes into a more fibroblastic phenotype. OSCC cells in the mineralized groups expressed more vimentin than non-mineralized, suggesting a phenotypic change compatible with epithelial-mesenchymal transition (EMT). Moreover, devices loaded with osteoblasts and osteocytes showed an increase in the proliferation and invasion of cancer cells with enhanced paracrine secretion of IL-6 and IL-8.

Conclusions

In conclusion, bone mineralization and the presence of osteoblasts and osteocytes in the matrix are correlated with EMT and a more invasive behavior in OSCC cells. These findings are crucial for understanding the mechanisms of bone invasion by OSCC, suggesting potential therapeutic targets directed at this interaction.

Injectable, Robust, Biocompatible Hydroxyapatite Nanoparticle Embedded Chitosan-Based Hydrogel with Potent Antibacterial Activity

Tapas Ghosh
PostDoctoral Scholar, Fugolin lab, OHSU School of Dentistry

Co-Authors: Sivashankari Rajasekaran and Ana Paula Fugolin

Introduction
Bacteria play a significant role in the development of serious oral pathologies, including periodontal disease. Periodontal disease (PD) is a chronic inflammatory condition that affects the tissues surrounding and supporting the teeth. Several strategies have been tested for the treatment and management of PD, but they are generally nonspecific, involve rapid and time-limited drug release, and are associated with invasive procedures. This leads to challenges in patient compliance. To address these limitations, we are proposing to design, synthesize and validate the first multimodal therapeutic hydrogel for a sustainable, local, and on-target management and treatment of PD.

Methods
In the first phase of this study, Fe/Zn co-doped hydroxyapatite nanoparticles a molar ratio of 0:0 (negative control), 0.05:0.05, 0.1:0.1, and 0.2:0.2 molar rations (FZHA-0, -1, -2, and -3, respectively) were synthesized and characterized by infrared spectroscopy, powder X-ray diffraction, thermogravimetry, and microscopic analyses. In the second phase, the chitosan-based hydrogel was synthesized through the cross-linking of chitosan (CS) with β-glycerol phosphate disodium salt (GP) at a physiological temperature. Briefly, 1.5-2% (w/v) CS was dissolved in a 0.1 M acetic acid solution under mild stirring conditions. Simultaneously, 60% (w/v) GP was dissolved in water and maintained at 4 °C, while the optimized concentration of Fe/Zn co-doped hydroxyapatite nanoparticles was prepared in water. This process involved adding the FZHA nanoparticles dispersion into the CS solution under constant stirring. Subsequently, the GP solution was gradually added dropwise into the FZHA/CS mixed solution to initiate the hydrogelation of FZHA-incorporated CS-GP (FZHA/CS-GP). As a control group, the bare CS-GP hydrogel was prepared using the same procedure, replacing the nanoparticle solution with distilled water. The test tube inverting method was used to measure the gelation time at constant temperature of 37 °C in a water bath. To analyze mechanical strength and other rheological properties of the CS-GP and FZHA/CS-GP hydrogel, rheology tests were performed. Morphologic characterization of the hydrogels was assessed by scanning electron microscopy. The FZHA/CS-GP will also be tested for in vitro swelling behavior and injectability, antibacterial activity by MIC assay. The data was statistically analyzed by one-way ANOVA and Tukey's test.

Results
The successful synthesis of FZHA nanoparticles was confirmed by XRD and infrared spectra. In PXRD spectrum of FZHA-0, the characteristic peaks of HA are observed at 32 and 39 degree and these peaks become broader as we increase the concentration of Fe and Zn. This observation is attributed due to the loss of crystalline structures of the HA nanoparticles. In FT-IR spectra, the peaks at 567, 602, 876 and 1039 cm-1 correspond to the stretching and bending frequency of PO_3^{4-} groups. The peaks at 1634 and 3492 cm-1 are assigned to the -OH stretching frequency of water. Morphological analysis highlighted the tendency of nanoparticle

agglomeration, primarily due to Oswald ripening. In relation to the rheological characterization of the hydrogels, the CS-GP hydrogel shows good viscoelastic nature and also displays good shear-thinning where the viscosity of the hydrogel gradually decreases with increase in the shear rate.

Conclusions

In conclusion, we have successfully synthesized and characterized the Fe/Zn doped hydroxyapatite nanoparticles. We have also developed β-glycerol phosphate crosslinked injectable CS hydrogel and encapsulated the synthesized nanoparticles into the hydrogel matrix. In our next plan, the antimicrobial activity and the biocompatibility of the nanoparticles encapsulated hydrogel will be screened. The successful outcomes from this works will allow us to develop a multifunctional injectable, inherent antibacterial hydrogel for the treatment of periodontal disease.

Immunostimulatory effects of Extracellular Membrane Vesicles From Oral Commensal Streptococcus sanguinis

Emily Helliwell
Senior Research Associate, Kreth lab, OHSU School of Dentistry

Co-Authors: Jens Kreth

Introduction

Streptococcus sanguinis is prevalent in the oral cavity and interferes with colonization of oral pathogens. Like other cell types, streptococci produce extracellular membrane vesicles, which contain specific molecular cargo and interact with host cells. Our goal is to define the particular immune response that S. sanguinis MVs have on eukaryotic cells, and find how this may differ from an immune response triggered by a pathobiont.

Methods

We used differential centrifugation methods coupled with image analysis to isolate and quantify S. sanguinis vesicles. Proteomic characterization of the vesicle cargo was done via mass spectrometry. To test the immunostimulatory effects, S.sanguinis vesicles were inoculated onto gingival epithelial cells, followed by gene expression analysis and gelatin zymography. Image analysis coupled with RNA quantification was used after dual inoculation of S. sanguinis and P. gingivalis MVs to determine cell viability.

Results

Proteomic characterization of the vesicle cargo identified several proteins predicted to influence host immune responses. Studies of gingival epithelial cells demonstrated that S. sanguinis MVs induced the production of IL-8, TNF-α, and Gro-α without causing cell death. Detailed inoculation studies showed dowregulation of gene expression of TLR4, Myd88 and MMP2 in a concentration-dependent effect on gingival epithelial cells. Gelatin zymography studies showed an increase in production of pro-MMP9 after inoculation by S. sanguinis MVs, however production of pro-MMP2 remained at a constant state. Pre-inoculation of gingival epithelial cells with S. sanguinis MVs prevented cell disassociation and death due to the presence of P. gingivalis MVs.

Conclusions

Our overall findings suggest that S. sanguinis MVs trigger an immune response on gingival epithelial cells, however this response is selective and suggests inhibition of some immune signaling pathways. Our results highlight an important role in commensalism; in which a microbe induces an immune response but avoids damage to host cells, thus discouraging infection by pathobionts.

An Enzyme-Responsive Nanoplatform for Preventing Collagen Degradation in Dental Tissues

Bao Huynh
Senior Research Assistant, Fugolin lab, OHSU School of Dentistry

Co-Authors: Tapas Ghosh, Sivashankari Rajasekaran, Ana Paula Piovezan Fugolin

Introduction
The collagen degradation mediated by host proteolytic enzymes, such as the metalloproteinases (MMPs), is strongly associated with the development of secondary caries at the restorative material-dental tissues interface and periodontal disease. Epigallocatechin gallate (EGCG) and quercetin are polyphenols with a potent MMP-inhibitory effect, but their incorporation in dental biomaterials remains as a challenge due to chemical incompatibility, poor diffusion, and limited substantivity. Therefore, this study is aimed at developing MMP-responsive nanomicelles loaded with EGCG and quercetin and assessing their stability and on-demand release.

Methods
The micellar nanoparticles consist of a block-copolymer conjugated with a peptide sequence which is recognized and cleaved by MMPs -2 and -9. For the block-copolymer synthesis, the compounds (N-Benzyl)-5-norbornene-exo-2,3-dicarboximide (1) and 1-{[(2S)-bicyclo[2.2.1]hept-5-en-2-ylcarbonyl]oxy}-2,5-pyrrolidinedione (2) were synthesized, then polymerized using a modified Grubbs catalyst. The final block-copolymer was precipitated in cold methanol, centrifuged, and characterized by NMR spectroscopy. The copolymer (50 mg/mL) was dissolved in an anhydrous mixture of dimethylformamide and dimethyl sulfoxide, along with the peptide sequence GPLGLAGGWGERDGS and N,N-Diisopropylethylamine (DIPEA) (1:4:16 copolymer:peptide:DIPEA). After stirring for 27 hr, the solution was precipitated in cold methanol, centrifuged, and the peptide-copolymer product characterized by NMR spectroscopy. To form EGCG/quercetin loaded micelles, the block copolymer-peptide (1 mg/mL), EGCG and quercetin (30 µM each) were dissolved in DMSO. Distilled water was added via syringe pump at 0.75mL/hr until critical micelle concentration (30% v/v aqueous). After 2 days of stirring, water was added via syringe pump at 5 mL/hr until reaching 50% v/v aqueous. The solution was transferred to dialysis tubing and placed in water (pH=8). The buffer was exchanged 3x per day for 2 days, then the procedure was repeated with Dulbecco's phosphate-buffered saline solution. The micelles were characterized by transmission electron microscopy (TEM), confocal microscopy, high-performance liquid chromatography (HPLC), dynamic light scattering (DLS), and zeta potential analysis. The responsivity to the MMP-9 was tested by incubating the micelles in a cleavage buffer for 24 hr at 37 °C, and analyzed by TEM, HPLC, DLS, and zeta analysis.

Results
The data were analyzed by one-way ANOVA and Tukey's test ($\alpha=0.05$). TEM micrographs showed the successful formation of spherical nanomicelles, with significant differences in electron density indicating clearly defined core and shell portions. Dynamic light scattering analysis revealed an average diameter distribution of micelles at 19.06 nm. Zeta potential results ranged from -37.5 mV to -43 mV, indicating strong nanomicelle stability regardless of the cargo composition. Confocal microscopy also revealed nanomicelles with a stable, unquenched core. Upon excitation at 488 nm, confocal imaging showed distinct nanomicelle cores exhibiting fluorescence from the encapsulated quercetin. Fluorescence spectroscopy efficiently confirmed

the encapsulation of quercetin but not that of EGCG, as its light absorbance overlaps with the nanomicelle shells. HPLC analysis has been employed as an alternative method and is currently ongoing. The responsiveness of the nanomicelles was confirmed through incubation with MMP-9, as evidenced by the morphological transition from round-shaped to a worm-like structure.

Conclusions

The synthesized nanomicelles proved to be a successful vehicle for encapsulation of MMP-inhibiting agents and other therapeutic drugs. The successful integration of peptides containing MMP recognition sequences is strong evidence for the potential of this platform to promote sustainable and on-demand drug delivery. In the next steps of this study, the biocompatibility of the platform will be assessed, along with the therapeutic efficiency of the platform at the adhesive interface and against periodontal disease using organ-on-chip devices and animal models.

The short-term effects of orthognathic surgery on condylar orientation and positions in bilateral sagittal split osteotomy patients

Laura Iwasaki (MS Thesis of Angela Li)
Professor and Chair, Oral & Craniofacial Sciences, OHSU School of Dentistry

Co-Authors: Angela Li*, Juliana Batista Melo da Fonte**, Saulo Sousa Melo*, Dongseok Choi^, Laura Iwasaki*, Jeff Nickel*
*Oral and Craniofacial Sciences, School of Dentistry, Oregon Health & Science University
**University of Campinas (UNICAMP), Sao Paulo, Brazil
^Biostatistics and Data Science, School of Public Health, Oregon Health & Science University

Introduction
Longitudinal studies have demonstrated that orthognathic surgery results in condylar resorption in >30% of cases. The current study aims were to: 1) analyze the angular and displacement changes of the condylar proximal segment in the three planes of space following surgery, and 2) estimate the post-surgical changes in compressive stress in response to a 9 N load.

Methods
In accordance with IRB oversight, pre- and post-surgical cone-beam computed tomography (CBCT) images were collected at one private oral surgery office. Inclusion criteria were individuals aged 15 years and older, without a history of craniofacial deformities, syndromes or temporomandibular disorders. Three-dimensional anatomical data were derived from pre- and post-surgical CBCT images. These data were used to analyze the post-surgical angular changes in the proximal segment in 3 planes of space. Additionally, three-dimensional pre- and post-surgical reconstructions of right and left TMJs were used to quantify minimum articular distances between the condyle and temporal bone. Changes in compressive stresses were performed using an empirical equation derived from laboratory tests of the effect of TMJ disc thickness on peak compressive stress for a 9 N load. ANOVA and mixed effects modeling were used to determine if there were significant pre- to post-surgical changes in proximal segment orientation and peak compressive stresses.

Results
Twenty-seven females and fourteen males provided complete records. Both the axial and sagittal planes showed significant (all $p < 0.05$) decreases in angulation after surgery. No change was found in the coronal plane. Average pre-surgical peak compressive stress of 0.18 (±0.01) MPa increased significantly ($p < 0.001$) to 0.27 (±0.02) MPa following surgery. Sagittal plane angulation changes were significantly related to changes in compressive stress ($p < 0.05$).

Conclusions
Efforts should be made during BSSO to maintain condyle orientation to prevent significant changes in peak compressive stresses.

Assessing obturation voids between radicular dentin and single cone gutta percha using CBCT in root canal prepared teeth.

Matt Jervis
Resident, Endodontics, OHSU School of Dentistry

Co-Authors: Dr. Karan J. Replogle, OHSU; Dr. Daniela Pita de Melo Department of Dentistry, Universidade Estadual da Paraiba, R. Baraúnas; Dr. Saulo Sousa Melo, OHSU;
Dr. Juliana B Melo da Fonte, DDS, MSD, PhD PGY-1, Oral and Maxillofacial Radiology University of Connecticut Farmington, CT

Introduction
Oral radiologists are often asked to identify the presence of voids in root canal obturation using CBCT. This is due to potential contribution to root canal failure that result from obturation voids. The voids allow space for fluid movement of nutrients for bacteria as well as space for biofilms and corresponding virulence factors to develop and result in apical periodontitis (1, 3). Determining these voids in CBCT is difficult due to beam hardening and blooming artifacts (10, 11). Micro CT is considered the gold standard of determining canal anatomy and determining accuracy of cleaning and shaping as well as obturation of canals (23). The aim of this study is to determine the level of intra and interexaminer accuracy and agreement in using CBCT to determine if a void is present between gutta percha and a root canal wall.

Methods
Twenty-five mandibular incisors with a single canal were decoronated using a diamond bur (Brasseler, USA) and prepared to 45.04 taper with K3xF rotary files (Kerr, USA) 1mm short of visible root apex (21, 22). This working length was recorded and single cone gutta percha (Dia-Dent, USA) of 45.04, 40.04, 35.04, 30.04, 25.04, 20.04, 15.04 were placed at length and scanned with i-CAT FLX VR 17 CBCT unit (Dental Imaging Technologies Corporation, USA). This resulted in an image total of 384 CBCT scans. Significant voids will be present in every cone except for the 45.04 cone as that is the prepared size of the canal. Micro-CT scans for 45.04 cone was completed to verify appropriate fit and provide the ground of truth for whether or not voids are present (Micro-XCT 200, USA). Two calibrated examiners viewed the 384 CBCT images and were asked to determine their level of certainty as to whether or not a void was present between the gutta percha cone and the canal wall in the mesial to distal dimension.

Results
The statistical analysis was performed. The tests included Kappa-Coefficient to determine intra and interobserver agreement, ANOVA, Tukey's post hoc test to find statistically significant differences between the observers' findings and whether or not an actual void was present and a ROC curve was produced to help determine sensitivity, specificity and accuracy of this assessment method. Results are pending. Initial impression of the data is that intra and interobserver agreement in determining voids between single cone gutta percha and root canal walls will likely be low.

Conclusions
Conclusions: Potential conclusion is that it CBCT does not show good sensitivity in detecting true voids between single gutta percha cones and root canal walls and that intra and interobserver agreement is also low.

Variable Polydispersity among beta-Crystallin Homodimers via Dynamic Light Scattering

Hayden Lackey
Student (R25 DORS intern), Lampi lab, OHSU School of Dentistry

Co-Authors: Hector Martinez, Kate Halverson-Kolkind, Larry David, Kirsten Lampi

Introduction
Crystallin aggregation invariably results in the formation of cataracts. Protein modification and unfolding are the primary factors that lead to aggregation. Crystallins that are less kinetically and thermodynamically stable are more likely to unfold and subsequently aggregate. The purpose of this experiment is to characterize the kinetic and thermodynamic stability of the $\beta B1$, $\beta B2$ and $\beta A3$ Crystallins using Dynamic Light Scattering.

Methods
Dynamic Light Scattering was used to determine the hydrodynamic radius of recombinantly expressed proteins by measuring light intensity fluctuation over time. The translational diffusion coefficient, calculated via the autocorrelation function, is inversely proportional to the hydrodynamic radius of the protein. proteins were recombinantly expressed and purified to >90% pure as measured by mass spectrometry.

Results
Our data also depicts differences in polydispersity among the β-Crystallins. Polydispersity measures the variance in the hydrodynamic radii distribution for a given sample. A larger polydispersity index is indicative of partial protein unfolding. Thus, polydispersity is an excellent metric for kinetic and thermodynamic stability. Our results showed that β-Crystallins B1 and A3 were significantly more polydisperse compared to β-Crystallin B2. β-Crystallin A3 in particular had a polydispersity index nearly 1.7 times that of β-B2 and a polydispersity distribution range close to twice that of β-B2.

Conclusions
Our findings suggest that β-Crystallins B1 and A3 are less kinetically and thermodynamically stable, implying a more primary role in aggregate and cataract formation in the human lens. These findings give direction to future experiments, most notably using native mass spectrometry, to give a more precise description of the thermodynamics, kinetics and specific protein-protein interactions involved in Crystallin aggregate formation.

Functionalization of glass surfaces for anti-biofilm properties for dental restorative materials

Luke Miller
Senior Research Associate, Pfeifer lab, OHSU School of Dentistry

Co-Authors: Miller, L.; Lucena, FS.; Wong, J.; Logan, MG.; Pfeifer, CS.

Introduction
Quaternary amines (QAMs) have been shown to have anti-biofilm properties when integrated into dental restorative composites. The alkyl chain length of the QAM is an important determinant for the desirable anti-biofilm properties of a material, but the literature can give conflicting requirements. This is in part due to the complex systems that the QAMs are integrated into, which typically consist of polymethacrylates with porous glass filler particles. In this study, glass surfaces are functionalized using small molecules and capped with QAMs of varying alkyl chain lengths.

Methods
Surfaces of acid-etched glass rods were functionalized with 3-(trimethoxysilyl)-propylamine followed by coupling with α-Bromoisobutyryl bromide to afford the halide initiator for atom transfer radical polymerization (ATRP). Polymers were synthesized with CuBr and 2-(dimethylamino)ethyl methacrylate. The terminal dimethyl amines were quaternized using alkyl halides with one (Q1), two (Q2), six (Q6), and sixteen carbons (Q16). Poly-DMAEMA (NoQAM) and poly-hexadecyl methacrylate (C16) were controls. S. Mutans strain UA159 growth was conducted in triplicate on the glass rods with each sample inserted on a 48 clear bottom well plate (TC treated) with 500 µL of a stock solution of TH media, 1% sucrose, and 1:500 dilution of an overnight inoculum. The growth was carried out for 24h, at low shaking, on a 5% CO_2 incubator. After 24h, the rods were carefully removed from the plates, washed three times with 1X PBS and the optical density (OD) of the planktonic bacteria was read at 600nm on a plate reader (SpectraMax iD3), then the discs were transferred to a 48 well plate with clear bottom and black edges, and the TH media was refreshed for each rod and the plate was incubated at a 5%CO_2 incubator for 90 minutes, then 5µL of Coelenterazine-h was added to each well and the luminescence was immediately read (at all wavelengths) to access the biofilm viability, afterward the rods were stained with 1% Crystal Violet solution and photographed with a stereomicroscope for qualitative analyses of the biofilm morphology. The biofilm on the surface of the rods was resuspended in 30% acetic acid solution for 20 minutes, then the discs were removed from the plate and the reading was performed at absorbance mode (562nm). Data was analyzed using one-way ANOVA or Kruskal-Wallis, with a significance level of 5%

Results
Q16 had the lowest value for optical density (0.1144 a.u.), followed by Q2 (0.2181 a.u.), and the remaining samples (NoQAM, Q1, Q6, C16) had statistically similar values of 0.2795, 0.2993, 0.2576, 0.2597 a.u. respectively. (p=0.007). For biofilm biomass, Q16 had a significantly lower absorbance (0.0519 abs) than the other samples (p<.001). Control C16 had a value of 0.2319 and control NoQAM and Q2 had statistically similar values of 0.3326 and 0.3387 respectively. Q1 and Q6 had the highest values of 0.03689 and 0.038095 respectively. As with the other results, Q16 stood out with the lowest biofilm viability measured by luminescence (1.25E1 RLU). Q2 was the next highest at 5.01E2 RLU. Q1, Q6, and C16 were similar with values of 1.8E3, 1.01E3 and 1.55E3 RLU respectively. NoQAM had the highest biofilm viability with a luminescence of 3.05E5 RLU.

Conclusions

In polymer composites for dental restorations, it can sometimes be difficult to elucidate the impact of a specific modification due to the nature of the complex mixtures. By functionalizing a glass surface, we can easily see the isolate the impact of a specific functionality. Glass surfaces were functionalized with QAM forming polymers and compared with functionalized surfaces without QAMs. Biofilms were then allowed to grow on the surfaces. Only the QAM with a sixteen-carbon chain was found to reduce the biofilm biomass. This simplified approach allows for easier evaluation and screening of functionalities for anti-biofilm properties.

The critical significance of Streptococcus mutans studies beyond UA159

Stephanie Momeni

Assistant Professor, Division of Biomaterials & Bioscience, OHSU School of Dentistry

Co-Authors: Madeline Krieger, CEDAR Knight Cancer Institute; Hui Wu, School of Dentistry

Introduction
Streptococcus mutans is a key etiological agent in early childhood dental caries (ECC). S. mutans UA159 is generally considered a model strain for caries; however, little is known about this strain's clinical prevalence. Clinical S. mutans UAB-10 strain has high prevalence among children with ECC and was recently reported to contain a novel butyrolactone-ladderane-like biosynthetic gene cluster (BL-BGC). The purpose of this study was to compare the genomic and transcriptomic variations between these two S. mutans strains.

Methods
Sub-cultured S. mutans UA159 and UAB-10 were grown in Todd Hewitt Broth (THB) at 37 C in 5% carbon dioxide and the DNA was extracted. Nanopore sequencing was used to obtain complete genomes. Comparative genomics were performed using the Anvio pipeline. For transcriptomics, subcultures were inoculated 1:1,000 in THB+1% sucrose and biofilms were grown for 16 hours. Three biological replicates were pooled and washed prior to RNA extraction. Transcriptomics library preparation, sequencing, and read mapping were performed by GenWiz. Transcriptomics analysis was performed using the DESeq2 package in R.

Results
The pangenome of S. mutans UA159 and UAB-10 contained 2,168 combined gene clusters.1,807 (83.3%) were core genes clusters found in both isolates. 361 were shell gene clusters found in only one strain (212 and 149 clusters were unique to UAB-10 and UA159, respectively). Of 2,037 total genes considered for transcriptomics analysis, 50% (1,027) of these genes were significantly different between the two strains (582 down-regulated, 446 up-regulated). Among genes unique to UAB-10 were the BL-BGC, a T7SS, and the toxin/antitoxin system yeeF/yezG.

Conclusions
Comparative genomics and transcriptomics demonstrate there are significant differences in these two clinically important S. mutans strains, even when grown in static culture. These fundamental distinctions highlight the crucial need to investigate other S. mutans strains beside UA159 to determine how clinical and epidemiologically supported S. mutans strains contribute to ECC.

A Pilot Study of TMD Pain and Nocturnal ANS Associated Masticatory Muscle Activity

Jeff Nickel

Professor, Division of Orthodontics and Dentofacial Orthopedics, OHSU School of Dentistry

Co-Authors: Brandon Zegarowski, Jeff Nickel, Hongzeng Liu, Laura Iwasaki, Department of Oral and Craniofacial Sciences, OHSU
Dongseok Choi, Department of Biostatistics & Data Science; OHSU
Yoly Gonzalez, Oral Diagnostic Sciences; State University of New York at Buffalo, Buffalo, NY, USA

Introduction
Pain associated with Temporomandibular Disorders (TMD) causes detrimental effects on daily function and quality of life of affected individuals. This pilot study tested for differences in autonomic nervous system and masticatory muscle activities in subjects with and without TMD-associated pain (±Pain). This project will test the following working hypothesis of whether or not:
1. There were significant differences in muscle duty factors between subjects with and without chronic pain.
2. There was a correlation between the independent variables i) ANS sympathovagal tone, ii) masticatory muscle duty factors, and the dependent variable of 6-month chronic pain intensity (CPI) scores.
3. There was a correlation between the independent ANS variables of i) sympathovagal tone, ii) parasympathetic activity, and the dependent variable of 6-month chronic pain intensity (CPI) scores.

Methods
According to IRB oversite, subjects were 18 years or older when enrolled. Subjects' levels of characteristic pain intensity (CPI) were assessed using validated instruments of the Diagnostic Criteria of Temporomandibular Disorders (DC/TMD). Subjects participated in two laboratory calibration sessions to quantify masseter and temporalis muscle activities per N of bite-force. Subjects were trained to use a portable electromyography (EMG) and electrocardiography (ECG) recorder, recording data for 3 nights, with each recording being greater than 6 hours. Characterization of nocturnal activity of the autonomic nervous system was accomplished using commercial software to quantify heart rate variability (HRV). Data of night-time ultradian cycling of sympathetic/parasympathetic tone for each night recording was fitted with a higher order polynomial. Peaks and valleys of ANS tone were identified based on the polynomial, and time (pNN50, parasympathetic activity) and frequency (sympathetic/parasympathetic, Low Frequency/High Frequency) domain measures of HRV were determined at inflection points. For these inflection points, muscle activities were quantified for activities ranging from >1 to <5 N of load on the mandible and represented as a % of total recording time. Analysis of variance (ANOVA) and post-hoc tests were used to determine if there were differences ($p < 0.05$) in muscle duty factors between ±Pain groups. Three-dimensional (3D) regression analysis tested for correlations between independent variables of ANS tone and muscle duty factor, and the dependent variable of CPI.

Results
Twenty-seven subjects completed the study protocols. Subjects with pain (+P) had significantly higher average muscle duty factors ($p < 0.02$) compared to subjects without pain (-P) subjects. There was a positive correlation ($R^2 = 0.75$) between muscle duty factors, sympathetic nervous

system activity, and CPI scores. The combination of independent variables of the ratio of sympathetic/parasympathetic activity (LF/HF), and parasympathetic tone (pNN50), showed a significant correlation ($R^2 = 0.67$) with pain scores.

Conclusions
1. There were significant differences in muscle duty factors at low-levels of jaw-loading between subjects with and without chronic pain.
2. There was a positive correlation between 6-month chronic pain intensity (CPI) scores versus masticatory muscle duty factors at low levels of jaw-loading and peak-to-valley ratios of sympathetic/parasympathetic activities (LF/HF)
3. There was a correlation between higher CPI scores versus lower parasympathetic activity (pNN50) and higher sympathovagal (LF/HF) activity.
.

Development of a versatile toolbox for genetic manipulation of Prevotella melaninogenica

Hua Qin
Senior Research Associate, Merritt lab, OHSU School of Dentistry

Co-Authors: Hua Qin1, Dustin Higashi1, Madeline Krieger2 and Justin Merritt1
1 Department of Oral Rehabilitation and Biosciences, OHSU School of Dentistry
2 Cancer Early Detection Advanced Research Center (CEDAR), Knight Cancer Institute, OHSU

Introduction

The Prevotella genus is comprised of Gram-negative obligate anaerobes, and is one of the most prominent genera in the human oral microbiome. Although emerging studies in humans have linked the increased abundance of Prevotella species to both oral and systemics disease as well as multiple cancers, our mechanistic understanding of Prevotella biology is rudimentary, largely due to potent genetic intractability throughout the entirety of the Prevotella genus. Despite our discovery of multiple intriguing host interaction phenotypes, further detailed mechanistic studies are inherently limited by intractable Prevotella genetics. In this study, we established an efficient genetic toolbox to manipulate Prevotella melaninogenica that will guide future genetic studies of its host-pathogen interactions.

Methods

Prevotella melaninogenica strains were isolated from clinical odontogenic abscess specimens on MCDC blood agar plates containing kanamycin and vancomycin. 16S rRNA genes sequencing was performed to verify the strains. PCR-assembled constructs were transformed into P. melaninogenica using natural competence.

Results

In this study, we isolated multiple Prevotella melaninogenica strains directly from clinical odontogenic abscess specimens and identified 2 strains exhibiting natural competence (exogenous DNA uptake). By exploiting this ability, we were able to obtain transformation efficiencies up to 2.65×10^{-6} using PCR product mutagenesis constructs assembled via cloning-independent methodologies. A negative selection system for P. melaninogenica was also established based upon induced sensitivity to the amino acid analog 4-chlorophenylalanine (4-CP). In addition, we successfully employed a codon-optimized version of the Green Renilla luciferase-encoding gene renG as a highly sensitive reporter gene in P. melaninogenica.

Conclusions

This study yields the first tractable genetic system in the Prevotella genus, which will provide new opportunities to systematically investigate Prevotella genetics, addressing a significant fundamental knowledge gap in the field.

Reinforcing Urea-Formaldehyde Microcapsules Stability through Additive Modulation

Sivashankari Rajasekaran

PostDoctoral Scholar, Fugolin lab, OHSU School of Dentistry

Co-Authors: Ana Paula Fugolin and Bao Huynh

Introduction

Urea-formaldehyde networks are widely utilized for encapsulating healing agents to repair microstructural cracks in dental restorative materials under thermal and masticatory stresses. While this approach holds promise for extending the clinical lifespan of dental restorations, it faces challenges related to physicochemical stability and potential formaldehyde cytotoxicity. In this study, we explore a novel approach by combining melamine and a high-toughness acrylamide additive, N,N-Dimethylacrylamide (DMAM), to enhance the physicochemical stability of poly (urea-formaldehyde) microcapsules (PUF) shells.

Methods

PUF microcapsules were prepared by the double emulsion method using mechanical stirring as the method of emulsification. The urea-formaldehyde shell was modified with different concentrations of melamine (0, 2.5, 5, 7.5 and 10%), encapsulating two different compositions of healing agents - 100%T (TEGDMA-Triethylene glycol dimethacrylate) and a combination of 80%T (TEGDMA) + 20%D (DMAM). Morphological characterization of the microcapsules was carried out by optical and scanning electron microscopies. The micrographs obtained were then utilized to calculate the average diameter using the ImageJ software. The reaction yield (%) was calculated after each reaction and the encapsulation efficiency (%) was assessed by acetone extraction method. The mechanical properties of the microcapsules were analyzed by nanoindentation method and the formaldehyde release from the shells was quantified by calorimetry using Purpald reagent. The data was statistically analyzed by one-way ANOVA and Tukey's test.

Results

The incorporation of melamine significantly impacted the shell's characteristics, making them rougher and more brittle as the melamine concentration increased. The reaction yield percentage ranged from 60 to 85%, and the average capsule size from 80 to 150 μm. Regarding nanoindentation results, the hardness values ranged from 0.15 to 4.4 GPa and the elastic modulus ranged from 2.1 to 4.4 GPa. Overall, the DMAM containing microcapsules showed increased hardness and decreased elastic modulus proving that microcapsules with DMAM exhibits more elastic and tougher behavior when compared to 100%T microcapsules. Quantification of formaldehyde emission from the microcapsules is ongoing. Overall, the most effective combination was achieved with the addition of both the high-toughness additive DMAM and 5% melamine.

Conclusions

The result of this study shows that the addition of high toughness compound DMAM and 5% melamine resulted in better microcapsules with respect to morphology, %yield and mechanical strength.

Unsaturated fatty acids impact the physiology and virulence of Streptococci

Jonah Tang
Research Assistant, Baker lab, OHSU School of Dentistry

Co-Authors: Jonathon L. Baker, Yujiro Hirose, Jan-Willem Veening, Victor Nizet

Objective & Methods
The order Lactobacillales encompasses some of the most important pathogens and commensals of the human microbiota including the streptococci, enterococci, and lactobacilli. Lactobacillales synthesize unsaturated fatty acids (UFAs) de novo via an isomerase enzyme, which is named FabM in *Streptococcus* and FabN in *Enterococcus*. Environmental stresses, including oxidative stress and acid stress, prompted an increase in the proportion of UFAs in the cell membranes of diverse Lactobacillales taxa including *Streptococcus gordonii*, *Streptococcus salivarius*, *Streptococcus mutans*, and *Lactocaseibacillus casei*. In S. mutans, specifically, these UFAs were crucial for survival against oxidative and acid stress, and inability to produce UFAs, via deletion of fabM, significantly reduced virulence of the organism in a rat model of dental caries. In this study, the role of fabM and UFAs in the physiology and virulence traits of *Streptococcus mutans, Streptococcus pyogenes* and *Streptococcus pneumoniae* was further explored.

Results
The loss of fabM and UFA production increased susceptibility of *S. mutans*, *S. pyogenes*, and *S. pneumoniae* to membrane-targeting antibiotics, antimicrobial peptides, acid stress, oxidative stress, and killing by human neutrophils to varying degrees.

Conclusions
Collectively, the data suggests that UFA production is crucial for persistence, immune evasion, and likely virulence, for these Streptococci with diverse methods of pathogenesis.

Tailoring material surface chemistry to control acquired pellicle composition

Fernanda Tsuzuki
PhD Student, Pfeifer lab, OHSU School of Dentistry

Co-Authors: Fernanda Lucena, Steven Lewis, Carmem S. Pfeifer

Introduction

Acquired pellicle (AP) is an acellular organic film formed on the tooth surface, consisting mainly of proteins and proteoglycans. The mature AP directs the initial adhesion of oral microorganisms to the tooth surface, providing specific receptors for bacterial adhesins, acting as a mediator of interactions between surfaces in the oral cavity (as well as dental materials) and biological agents in the mouth. Therefore, the aim of this study was to investigate how the surface chemistry of polymeric materials, specifically the hydrophilic character, influence the proteomic composition of the AP and biofilm subsequent attachment.

Methods

BISEMA (hydrophobic) and PEGDMA (hydrophilic) either alone or combined at a 1:1 ratio (100/0; 50/50; 0/100 wt%) were used to make discs and then treated with human saliva for 2h. For proteomic evaluation, the salivary proteins from the AP were removed from the surface of the discs by rubbing schrimer strips, then separated by SDS-PAGE and samples were injected into the QEHF mass spectrometer. The surface chemistry was characterized by contact angle (WCA) and infrared spectra of surfaces were obtained with ATR spectroscopy to evaluate degree of conversion (DC). ATR was also used to quantify surface protein content by subtracting the spectra from the naïve and the protein-adsorbed specimen using the Amide I peak (1651-1655 cm-1- Origin software). The viability of S. mutans biofilms was evaluated by bioluminescence (Luciferase Assay) and Crystal Violet (CV) with or without AP present. The bacterial activity was also analyzed using microcosms biofilm model from patient plaque inoculum and maturation of biofilm for 72 h. The DNA of the microorganisms present in the biofilm formed on the AP was isolated using the ZymoBIOMICS DNA Miniprep kit (Zymo Research), using a double-elution protocol with 50 μl of H2O at 60°C and significant differential taxa abundance was determined using LEFSe trough the microbiomeMarker package (LDA value cutoff of 1, Kruskal-Wallis and Wilcoxin cutoff of .05). WCA, DC, bioluminescence and biomass data were analyzed by two-way-ANOVA (factors:material composition and presence of AP) and Tukey's test for multiple comparisons (α=0.05).

Results

The WCA ranged from 74.5±1.9 to 47.6±2.9, for BisEMA and PEGDMA, respectively (p<0.001). The more hydrophilic materials showed a higher concentration of -OH (3400cm-1) and Amide-I (1650cm-1) peaks. Proteomic analysis identified more than 415 proteins. The increase in the Amide I peak detected by ATR analysis on the surface of the more hydrophilic samples showed greater protein adsorption on these discs. The protein composition for PEGDMA was similar to that of saliva, but with marked differences between the materials. BisEMA disks were enriched with Desmoplakin, Desmoglein-1, Junction plakoglobin, and Filaggrin-2, whereas PEGDMA disks were enriched with Desmoplakin, polymeric immunoglobulin receptor, alpha-amylase 1B, and mucin-5B. The presence of AP influenced the results of biofilm viability (p<0.001) and biomass (p=0.007). Microcosm DNA analysis showed greater enrichment of S. mutans, Veionella, S. vestibularis and S.anginous in BisEMA discs.

Conclusions

The results demonstrate that the polymer surface chemistry does influence the proteomic composition of the AP and even relatively subtle differences in polymer composition can affect the proteomic profile and subsequence biofilm adherence. This proof-of-concept results have shown that it is possible to rationally design materials that control AP formation and will be utilized to design surfaces that can ultimately tailor the ecology of the biofilm on surfaces in the oral cavity.

Assessing obturation voids between radicular dentin and single cone gutta percha using a novel photon counting intraoral sensor.

Erin Waid
Resident, Endodontics, OHSU School of Dentistry

Co-Authors: Saulo Sousa Melo, DDS; Karan Replogle, DDS; Daniela Pita de Melo, DDS

Introduction
The aim of this study is to determine the level of intra and interexaminer accuracy and agreement in using a novel photon counting sensor versus a traditional intraoral sensor to determine if a void is present between gutta percha and a root canal wall.

Methods
Twenty-five mandibular incisors with a single canal were decoronated and prepared to 45.04 taper with K3xF rotary files (Kerr, USA) 1mm short of visible root apex. This working length was recorded and single cone gutta percha (Dia-Dent, USA) of 45.04, 40.04, 35.04, 30.04, 25.04, 20.04, 15.04 were placed at length and imaged with a novel photon counting sensor and traditional intraoral sensor. A total of 576 images were captured. Significant voids will be present in every cone except for the 45.04 cone. Micro-CT scans for 45.04 cone were completed to verify appropriate fit and provide the ground of truth for whether or not voids are present (Micro-XCT 200, USA). Four calibrated examiners viewed these 576 images. Observers were asked to determine their level of certainty as to whether or not a void was present between the gutta percha cone and the canal wall.

Results
The statistical analysis including Kappa-Coefficient to determine intra and interobserver agreement, ANOVA, Tukey's post hoc test will be performed to find differences between the observers' findings and whether or not an actual void was present and a ROC curve was produced to help determine sensitivity, specificity and accuracy of this assessment method.

Conclusions
to be determined

Use of Dental Adhesives to Improve Bond Strength of Titanium Implants to Bone

Samuel Weber
Research Engineer, Pfeifer lab, OHSU School of Dentistry

Co-Authors: S. S. Patty, M. G. Logan, S. H. Lewis, J. L. Ferracane, C. S. Pfeifer

Introduction
The underlying complications involved in biomedical device implantation are recurrent infection and loss of retention at the body-device interface. Commercial dental adhesives were combined with PMMA based bone cements to improve shear bond strength between bone and titanium implants, after cycling under physiologically relevant conditions.

Methods
Commercial dental adhesives ranging from 4th-7th Generation (Scotchbond Multi-Purpose – SBMP, 3M, Single Bond Plus - SB, 3M, Clearfil SE Bond – CFSE, Kuraray, Scotchbond Universal Plus – SBU, 3M) were applied to bone and cured at 1400 mW/cm2 before combining with PMMA bone cement materials (Jet Acrylic, Lang Dental and Arthroplasty Bone Cement R, BC, Biomet) to form the bonding interface between bone and a 6 mm diameter Ti implant. Shear bond strength was assessed at a speed of 1.0 mm/min after storage in MilliQ water for 24hrs and post 1-week mechanical cycling. SEM was used to image the bond interface and layer thickness. Quantitative data was analyzed with two-way ANNOVA/Tukey's test (alpha=5%).

Results
SBS values for all materials after water storage or mechanical cycling are shown in the Table. The use of dental adhesives led to 15 to 20-fold increase in bond strength, with the self-etch system (Clearfil SE Bond) showing the greatest improvement after storage in water or after cycling in the bioreactor. Mechanical cycling led to a slight decrease in bond strength for all materials but that was still 10 to 15-fold greater than the control.

Conclusions
This study demonstrates that applying dental adhesives prior to the PMMA bone cement materials can help increase retention at the body-device interface.

Visualizing and monitoring pH in Veillonella and Streptococci biofilms using HaloTag

Zhengzhong Zou
Senior Research Associate, Wu lab, OHSU School of Dentistry

Co-Authors: David Anderson; Justin Merritt

Introduction

Veillonella plays a significant role in the human oral microbiome but can transform into an opportunistic pathogen. Its presence correlates with severe early childhood caries, intraradicular infections, and periodontitis. Veillonella has shown the ability to coaggregate with Streptococci, Actinomyces, Fusobacterium, and Porphyromonas, facilitated by outer membrane adhesins. To gain a deeper understanding of Veillonella's bridging role in oral biofilms, we conducted a proteomic analysis of Veillonella parvula SKV38's outer membrane. Additionally, we developed HaloTag Biosensors to monitor pH and metabolic changes in multi-species oral biofilms featuring Veillonella.

Methods

We employed both surface-shaving and biotinylation methods to extract surface proteins of V. parvula SKV38. In the surface-shaving method, live bacterial cells were digested for 30 min with trypsin. In the biotinylation method, intact cells are treated with sulfo-NHS-SS-Biotin, to which the cell membrane is impermeable. Subsequently, labelled proteins were separated from non-labelled proteins by affinity chromatography with neutravidin. Peptides separation and identification were performed by high-performance liquid chromatography combined with tandem mass spectrometry (LC-MS/MS). Codon optimized HaloTag were tagged to the C terminus of FNLLGLLA_00042, the passenger domain of autotransportor ehaG_1 in V. purvula SKV38 and the variable region of SpaP in Streptococcus mutans UA159 respectively. For cellular imaging, we used cell permeant HaloTag Fluorescent ligand TMR and impermeant ligand Alexa Fluor® 488. HaloTag® AcidiFluor™ Orange Ligand, a live cell imaging probe for acidic pH, was employed for monitoring biofilm pH.

Results

The integration of bioinformatics and proteomics results allowed the identification at least 45 out membrane proteins, including 9 autotransporter adhesins, 3 lipoproteins, 3 peptidases, 2 OmpH family proteins, 4 out membrane factor family proteins, 2 cellulosomes-anchoring proteins, 10 transporters and 12 uncharacterized proteins in V. parvula SKV38. Notably, 4 autotransporters (UpaG_1, UpaG_2, EhaG_1 and Ata_2) and an uncharacterized protein FNLLGLLA_00042 within the autotransporter adhesin gene cluster exhibited high spectra counts. All HaloTag-fused proteins, including EhaG_1::HaloTag and FNLLGLLA_00042::HaloTag in V. parvula, as well as SpaP::HaloTag in S. mutans, were visualized with cell permeant ligand TMR or the impermeant ligand Alexa Fluor® 488. Among these, FNLLGLLA_00042::HaloTag showed the strongest signals.

Conclusions

Both the surface-shaving and biotinylation methods proved effective in extracting surface proteins from Veillonella, with minimal contamination by cytoplasmic proteins. We successfully adapted the HaloTag technology for use in S. mutans and V. purvula. The cell impermeant ligand Alexa Fluor® 488 demonstrated excellent performance in surface protein detection, offering rapid labelling and high specificity. Our next step involves applying HaloTag®

AcidiFluor™ Orange Ligand to monitor pH changes in multi-species biofilms containing Veillonella and Streptococci.

Research Day
2024

Poster Session #2 *(Evens)*

10:10am-11:40am

Thursday, March 7

Robertson Life Science Building, Portland, OR

OHSU

SCHOOL OF DENTISTRY

Research Day

Poster Session #2 (Evens) – Posters and Abstracts Alphabetical by Presenter's last name
Note: CaseCATs do not have associated Abstracts.

Name	Poster Number	Category	Title
Philopater Badawi	28	DMD STUDENT	Performance of a Novel Dental X-ray Sensor in the Assessment of Caries-like Lesions
Despoina Bompolaki and Christina Truong	8	FACULTY	YouTube as a learning tool in dental education: student and faculty perspectives
Molly Forde	14	RESIDENT	Pre-Operative Management of Pediatric Dental Patients Awaiting Full Mouth Dental Rehabilitation Under General Anesthesia
Cristiane Franca	26	FACULTY	Perivascular Mural Cells Regulate Vascular Function in Stiff Cancer-Associated Tumor Microenvironment On-a-chip
Kate Halverson-Kolkind	40	STAFF	Deamidation increases the rate of disulfide bond scrambling in glutathionylated gammaS-crystallin
Dustin Higashi	4	STAFF	The Parvi-Paradox. Studies on Parvimonas micra-Neutrophil interactions reveal insights into the pathogenesis of an oral pathobiont.
Laura Iwasaki (MS Thesis of Brandon Nguyen)	6	FACULTY	The effect of mandibula protrusion on pediatric temporomandibular joint stresses and association with mandibular growth
Daniel Kim and Daniel Chen	54	CaseCAT	The Impact of Fusobacterium nucleatum Modulation on Colorectal Cancer Treatment
Jay Kim	20	RESIDENT	Evaluating Patient Behavior Pre-operatively and Post-operatively Following Dental Treatment Under Moderate Sedation and General Anesthesia: A Retrospective Review
Jack Klar and Dominic Delgado	58	CaseCAT	Implant retained overdentures as the standard of care for the edentulous mandible
Ryan Knapp; Aaron Bell; Gregg Smith	50	CaseCAT	The Effects of Micro-osteoperforations on Rate of Space Closure in Orthodontic Tooth Movement in Adult Patients
Steven Lewis	30	STAFF	Rapid FTIR-ATR Spectroscopic Imaging for Analysis of the Dentin/adhesive Interface
Matthew Logan	16	FACULTY	Design and validation of a co-polymerizable MMP inhibitor
Fernanda Lucena	12	POSTDOC	Nanomolar inhibitor of MMP activity for hybrid layer preservation
Maria Eduarda Marinho	34	PhD STUDENT	Salivary biofilm complex model to evaluate bacterial activity in dental materials
Molly McCoy and Narita Narkhede	52	CaseCAT	The Impact of Fluoride on Titanium Implants
Rong Mu	22	STAFF	Investigating diadenylate cyclase (DAC) and protein-protein interactions in Streptococcus mutans
Jonathan Nguyen	18	DMD STUDENT	Anaerobic Protein Expression in Benign vs. Malignant Head and Neck Tumors: a Pilot Study
Peter Nguyen	46	DMD STUDENT	Self-Sterilizing Surfaces Using Quaternary Ammonium Methacrylates and its Zwitterion
Jeff Nickel	34	FACULTY	Autonomic Function and Muscle Activity in Growing Children
Ahmad Oubaid	44	RESIDENT	The Impact of the American Dental Association Antibiotic Prescribing Guidelines on prescribing practices within a Dental School Setting
Clara Park	2	DMD STUDENT	Antimicrobial oligomeric additives for dental adhesives and composites
Sarah Patty	32	STAFF	Central Venous Catheter Modifications with Covalently Anchored Antimicrobials & Antithrombogenics for Biofilm Inhibition: proposed project
Edward Pham	24	RESIDENT	The Effect of Social Stories on Children's Behavior in a Pediatric Dental Clinic: A Pilot Study
Genevieve Romanowicz	42	POSTDOC	Vascularized Bone-like Organoids: A Model System And Regenerative Strategy
Mauricio Sousa	36	POSTDOC	Fusobacterium nucleatum drives tumor-associated macrophage-like cells in an engineered oral squamous cell carcinoma on-a-chip
Aleya Steckel and Valerie Truong	56	CaseCAT	Utilizing TADs in Conjunction with Clear Aligners to Distalize Maxillary Molars in Patients with Class II Malocclusion
Tiffany Tep	48	CaseCAT	Overview of Treatment Modalities for Pre-Eruptive Intracoronal Resorption (PEIR)
Jade Wong	10	STAFF	Mechanistic study of the antibiofilm effect of QAM-based materials

OHSU

Performance of a Novel Dental X-ray Sensor in the Assessment of Caries-like Lesions

Philopater Badawi
DMD Student, OHSU School of Dentistry

Co-Authors: Juliana B. Melo da Fonte, Division of Oral & Maxillofacial Diagnostic Sciences, University of Connecticut; Daniela Pita de Melo, State University of Paraiba, Brazil; Ana Paula Piovezan Fugolin, Department of Oral Rehabilitation and Biosciences, OHSU SOD; Saulo L. Sousa Melo, Department of Oral and Craniofacial Sciences, OHSU SOD

Introduction

Photon counting (PC) sensors are capable of discriminating X-ray photon energies by a direct conversion of X-ray photons into electrical charges. This technology ensures the stability of image acquisition and eliminates the interference caused by light scattering which inherently happens in CCD/CMOS sensors commonly used in Dentistry. Given that PC sensors are becoming rightly available for dental imaging, the aim of this study was to compare the diagnostic performance of an intraoral PC sensor in comparison to 2 CMOS sensors in the assessment of caries-like lesions.

Methods

Sixty extracted human teeth (30 premolars and 30 molars) extracted for therapeutic reasons unrelated to the present research were selected. A demineralizing solution including 2.2mMol $CaCl_2$, 2.2mMol $NaH_2 PO_4$, 50mMol acetic acid, and pH set at 4.5 was used to induce caries-like defects on the distal surface of 15 premolars (dPM) and the mesial surface of 15 molars (dM). The remaining 15 sound premolars (sPM) and 15 sound molars (sM) were kept caries-free. Phantoms consisting of 4 posterior teeth were mounted such that the second premolar and first molar sockets were used to place the sample in 4 different combinations: dPM-dM, dPM-sM, sPM-dM, and sPM-sM. Standardized radiographs were obtained with two CMOS sensors (RVG and Dexis) and one PC sensor (XpectVision). All images were coded and randomly shown to three previously calibrated dentists. Their evaluations of the presence or absence of caries-like lesions were scored using a 5-point rating scale. Observers' agreement was verified through Cohen's kappa. Sensitivity, specificity, accuracy and area under the ROC curve (AUC) were calculated and verified through ANOVA and Tukey test. The significance level was set at 5%.

Results

The intraobserver agreements varied from fair to perfect agreement (RVG: 0.676-0.871; Dexis: 0.643-1; XpectVision: 0.328-1) and the interobserver agreements varied from fair to almost perfect agreement (RVG: 0.615-0.786; Dexis: 0.685-0.848; XpectVision: 0.353-0.604). The tested sensors presented values of specificity (70.57-83.35), accuracy (64.98-71.10), and area under the ROC curve (72.63-78.00) with no statistically significant differences ($p>0.05$). On the other hand, PC sensor presented higher sensitivity values in comparison to the CMOS sensors and that difference was statistically significant when the PC sensor was compared to the RVG sensor (PC Sn = 66.12 vs. RVG Sn = 49.45, p=0.017). When comparing the diagnostic performance while assessing different teeth (dPM and dM) within the same sensor, sensitivity was higher for dPM on all sensors (RVG, p = 0.001; Dexis, p = 0.003; XpectVision, p = 0.039) and AUC values were higher for dPM on a CMOS sensor (Dexis, p=0.008) and PC sensor (p=0.037).

Conclusions

Under the studied test conditions, the performance of the PC sensor was not only similar to that of the more commonly used dental sensors, but also slightly superior in diagnosing caries-like lesions when those were truly present (i.e. sensitivity).

YouTube as a learning tool in dental education: student and faculty perspectives.

Despoina Bompolaki
Associate Professor and Director, Clinical Dental Practice, OHSU School of Dentistry

Christina Truong
Assistant Professor of Restorative Dentistry, OHSU School of Dentistry

Co-Authors: Marina Youssef DMD Candidate, Class of 2024

Introduction
Online video sharing platforms have become integral parts of students' daily lives, providing a vast array of information and educational resources. Dental students, in particular, often turn to these platforms to supplement their education, seeking to acquire new skills or gain a deeper understanding of concepts covered in their restorative and dental foundation courses. The purpose of this study was to assess the usage of the most popular online video sharing platform (YouTube) among predoctoral dental students, as well as present student and faculty perspectives on using YouTube as an adjunct of their preclinical and clinical education.

Methods
Electronic (Qualtrics) surveys were distributed to all predoctoral dental students (DS1 - DS4) and full-time faculty members at Oregon Health & Science University School of Dentistry. Participation in the survey was voluntary and anonymous. Before distributing the surveys to the entire sample, a pilot study was performed (including 10 students and part-time faculty), to increase survey validity and reliability. Data collected via the surveys were analyzed using SPSS Statistics.

Results
Thirty-nine faculty (20 male, 19 female) and 42 students (26 male, 15 female, 1 other) completed the online survey. The majority of faculty (79.5%) and students (88.1%) visit YouTube at least once weekly. A very small percentage (2.6%) of faculty, as opposed to a larger percentage of students (26.2%), stated they use YouTube to watch educational videos related to dentistry ($p = 0.002$). Faculty are more likely to recommend specific YouTube videos to students during preclinical education (first and second year), but less likely to do so during clinical education (third and fourth year). Most faculty and students stated that the ideal duration of an educational video is 10 minutes or less. Overall, faculty had a worse perception of YouTube as an educational tool, as compared to students.

Conclusions
Given the widespread use of YouTube for educational purposes, this study is significant in assessing its effectiveness as a learning resource in dental education. The findings of this study could significantly influence the integration of digital media in dental education, potentially leading to the development of guidelines for the use of YouTube as a supplementary educational tool. It may also prompt the creation of more peer-reviewed, reliable content on YouTube by dental educators, enhancing the quality of information available to students globally.

Pre-Operative Management of Pediatric Dental Patients Awaiting Full Mouth Dental Rehabilitation Under General Anesthesia

Molly Forde
Resident, Pediatric Dentistry OHSU School of Dentistry

Co-Authors: Dongseok Choi, PhD OHSU-PSU School of Public Health

Introduction
To investigate the pre-operative management of pediatric dental patients who are awaiting full mouth dental rehabilitation (FMDR) under general anesthesia (GA) and examine the types of non-surgical interventions utilized.

Methods
Study was approved by OHSU IRB (IRB #00025556). An electronic survey was sent to 6,943 individuals who are current members of the American Academy of Pediatric Dentistry (AAPD). Questions included basic demographic data such as years of experience, geographic location, and type of clinical setting practiced in. Additional questions included questions that detailed current wait times for dental surgery under GA, frequency of follow-up for patients awaiting surgery, and frequently used non-surgical techniques. All responses were recorded via the survey platform Qualtrics. Exploratory data analysis completed included descriptive statistics and frequency tables. Fisher's exact test was utilized to test the association between patient wait time and treatment setting (hospital vs outpatient surgical center or in-office).

Results
An electronic survey was sent to 6,943 individuals who are current members of the American Academy of Pediatric Dentistry (AAPD). A total of 598 responses were collected, with 393 participants meeting the selection criteria, resulting in a response rate of 5.8%. Of the practitioners that responded to the survey, 80% worked in private practice in some capacity. There was a statistically significant difference in the current wait time for patients being treated in a hospital setting versus an outpatient surgical center or in-office GA, with the wait time being shorter in an outpatient surgical center or in-office GA. The most frequently accepted non-surgical intervention among all types of clinical settings was the application of silver diamine fluoride (72%). Additionally, SDF was also the most accepted non-invasive technique across all geographic locations. Hall-Crown placement was the least commonly accepted non-invasive technique (or tied for the least accepted) across all clinical settings and in all geographic regions. Commonly reported barriers to the use of these non-surgical interventions included the extent of the carious lesions rendering these non-surgical interventions non-effective or detrimental (74%) and the patient's cooperation inhibiting their use (72%).

Conclusions
For pediatric patients and those with SHCN requiring dental treatment under GA, the wait time is less for surgery in an outpatient or in-office GA setting compared to a hospital. Across all clinical settings, application of SDF is the most accepted non-surgical technique in the pre-operative management of patients awaiting treatment under GA, while HT is the least accepted. Commonly cited barriers to the use of non-surgical interventions in the management of patients awaiting treatment under GA include the extent of the carious lesions rendering these interventions non-effective or detrimental as well as the patient's cooperation/behavior inhibiting their use.

Perivascular Mural Cells Regulate Vascular Function in Stiff Cancer-Associated Tumor Microenvironment On-a-chip

Cristiane Franca
Research Assistant Professor, Division of Biomaterials & Biomedical Sciences,
OHSU School of Dentistry

Co-Authors: Maria Elisa Lima Verde1,2,3, Alice Sousa1,2,3, Amin Mansoorifar1,3, Avathamsa Athirasala1,2,3, Rahul Visalakshan1,2,3, Anthony Tahayeri1,2,3, Jennifer Bays4,5, Marina Uroz4,5, Christopher Chen4,5, Luiz E. Bertassoni1,2,3,6,7,8

1. Knight Cancer Precision Biofabrication Hub, Knight Cancer Institute, OHSU; 2. Cancer Early Detection Advanced Research Center (CEDAR), Knight Cancer Institute, OHSU; 3. Department of Oral Rehabilitation and Biosciences, School of Dentistry, OHSU, Portland, OR 97201, USA
4. Biological Design Center, Department of Biomedical Engineering, Boston University; 5. Wyss Institute for Biologically Inspired Engineering, Harvard University, Boston, MA 02215, USA;
6. Division of Oncological Sciences, School of Medicine, OHSU; 7. Department of Biomedical Engineering, School of Medicine, OHSU; 8. Center for Regenerative Medicine, OHSU.

Introduction
The transition of a healthy tissue to malignant cancer is characterized by a marked increase in extracellular matrix deposition and collagen density. Despite the large body of work on endothelial cell changes in tumor angiogenesis, little is known about the dynamic interactions of endothelial cells, perivascular cells, and the extracellular matrix in early-to-late stage cancers. We hypothesize that stiffness sensing of vasculature is mediated mostly by perivascular cells.

Methods
To model the spectrum of vascular changes occurring early to late cancers, we developed an organ-on-a-chip model of pericyte-supported capillaries with collagen having increasingly higher density, stiffness and discrete fibril microarchitectures. Briefly, 160-um channels were engineered using type I collagen that underwent fibrillogenesis at different temperatures (4, 16, 21, and 37°C), resulting in a soft reticular network, consistent with pre-cancerous vascular capillaries, and stiff fibrillar networks, consistent with tumoral vascular capillaries.

Results
Vascular capillaries engineered in matrix microenvironment consistent with a healthy non-fibrotic tissue, showed more pericyte differentiation ($p < 0.05$), endothelial cell junctions ($p < 0.05$), and effective barrier function. In contrast, vessels engineered using stiffer fibrillar collagen, consistent with a cancer-like extracellular microenvironment, was associated with uncontrolled cell migration, vascular leakiness, impaired basement membrane composition, and higher RNA expression for interleukin 8 (IL8), TP53, TGFbeta and vimentin, thus suggesting a system that compatible with the spectrum of tumoral vasculature changes in cancer lesions. Such patterns were only observed in vessels engineered with perivascular mural and ECs cells, and not with ECs only. Silencing of TGFbeta or Notch3 in mural cells, independently of ECs, re-established a healthy vascular morphology and function.

Conclusions
Perivascular cells have a major effect in sensing the differences in collagen architecture and guiding vessel integrity, thus pointing to a novel (and possibly better) target for antiangiogenic therapies.

Deamidation increases the rate of disulfide bond scrambling in glutathionylated gammaS-crystallin

Kate Halverson-Kolkind
Research Assistant, Lampi lab, OHSU School of Dentistry

Co-Authors: Wheeler, S. Thorn, D.C., David, L.L., Lampi, K.J.
Chemical Physiology and Biochemistry

Introduction
Deamidation and glutathionylation of cysteines in crystallins are two major age-related modifications associated with cataract formation. The purpose of this study was to test whether deamidation increases the rate of disulfide exchange between glutathionyled cysteines in gammaS and buried cysteines when gammaS is partially unfolded in guanidine.

Methods
Wild type (WT) gammaS and triple mutant (TM) gammaS containing N14D, N76D, and N143D deamidation mimics were glutathionylated by incubation at 1.6 mg/ml concentration in 2 mM oxidized glutathionine (GSSG) in 20 mM phosphate, 150 mM NaCl, 1 mM EDTA (pH 7) for 48 hours at 37°C. Disulfide exchange between sites of glutathionylation and buried cysteines was then initiated by addition of 2.75 M guanidine and incubation at 30°C between 0.5-10 min. Loss of glutathione and introduction of disulfide bonds was determined by measuring whole protein masses using mass spectrometry. Experiments were performed in triplicate using two different preps of purified WT and TM gammaS.

Results
Both WT and TM gammaS undergo a single glutathionylation and single disulfide bond introduction when incubated in 2 mM GSSG for 48 hours. Our previous studies showed that incubation in 2.75 M guanidine causes more rapid unfolding of TM gammaS than in WT gammaS. Treatment of glutathionylated gammaS under these conditions also causes a more rapid loss of glutathione. TM loses 60% of its glutathione after 1.5 min in 2.75 M guanidine, while WT gammaS loses only 40%. There were statistically significant differences in the rate of glutathione loss between WT and TM gammaS at 1, 1.5, and 2.5 min of unfolding in 2.75 M guanidine ($p<0.03$). Heating glutathionylated WT and TM gammaS at 60°C also initiates glutathione loss, but unlike guanidine treatment, causes precipitation of gammaS, while non-glutathionylated gammaS does not precipitate.

Conclusions
Introduction of deamidations in gammaS resulted in more rapid disulfide exchange reactions in the protein due to its greater susceptibility to denaturation in guanidine. Glutathionylation is known to occur in aged cataractous lenses. Deamidation may destabilize gammaS and result in transient exposure of internal cysteines that undergo disulfide exchange at glutathionylation sites, locking the protein into non-native conformations that then precipitate. This model system will allow more thorough examination of this process and investigation of the role of both deamidation and oxidation in cataract formation.

The Parvi-Paradox. Studies on Parvimonas micra-Neutrophil interactions reveal insights into the pathogenesis of an oral pathobiont.

Dustin Higashi
Research Associate, Merritt lab, OHSU School of Dentistry

Co-Authors: Hua Qin, Zhengzhong Zou, Elizabeth A. Palmer, Jens Kreth, and Justin Merritt

Introduction
Parvimonas micra is a pathobiont from the oral cavity that is strongly associated with mucosal dysbiotic disease, as well as multiple types of cancer. Inflammation is a hallmark of a number of oral diseases such as periodontitis and dental abscess, and corresponds to an influx of neutrophils (PMNs) to sites of infection. PMNs play a major role in the clearance of pathogenic microbes as well as in immune system homeostasis. Despite the presence of PMNs at sites of these oral diseases, P. micra levels are actually enriched. We hypothesize that P. micra have evolved the ability to circumvent destruction by PMNs.

Methods
PMNs were isolated from peripheral blood of healthy human subjects and ex vivo infection studies with P. micra were performed. We determined PMN phagocytic capacity using high-resolution microscopy as well as gentamicin protection assays. We further investigated the PMN response to P. micra exposure using flow cytometry and ELISA to measure cell viability and degranulation. Bacterial survival was determined using plating assays.

Results
P. micra is able to survive in the presence of, and within PMNs while not impacting PMN viability. P. micra infection induces a modest level of degranulation in PMNs. Phagocytosed P. micra avoid fusion with intracellular granules.

Conclusions
Our findings provide early insights into how P. micra is able to thrive in the inflammatory environment of the host.

The effect of mandibula protrusion on pediatric temporomandibular joint stresses and association with mandibular growth

Laura Iwasaki (MS Thesis of Brandon Nguyen)
Professor and Chair, Oral & Craniofacial Sciences, OHSU School of Dentistry

Co-Authors: Brandon Nguyen*, Ying Liu**, Hongzeng Liu*, Saulo Sousa Melo*, Jeff Nickel*, Laura Iwasaki*
*Oral and Craniofacial Sciences, School of Dentistry, Oregon Health & Science University
**Epidemiology and Biostatistics, College of Public Health, East Tennessee State University

Introduction
In a pediatric population before orthodontic treatment, to determine if there were: 1. significant differences in A. predicted TMJ loads (% applied bite force (BF)) and B. estimated TMJ compressive stresses (σ, MPa) during unilateral biting on molars with the mandible in retruded position compared to on molars and incisors with the mandible protruded to class I occlusion; and 2) correlations of A. predicted TMJ loads and B. estimated TMJ compressive stresses with dependent variables of sex, age, mandibular plane angle, ramal length, and/or mandibular length.

Methods
According to OHSU Institutional Review Board oversight, subjects were enrolled based on inclusion criteria: age 10-14 years; skeletal Class II malocclusion with treatment plan for fixed orthopedic appliance therapy to promote mandibular growth; permanent teeth erupted with, at a minimum, permanent incisors and first molars present; cervical vertebral maturation stage 2-3; and exclusion criteria: history of TMJ trauma, musculoskeletal disease, or craniofacial anomaly; teeth with conditions that would impair participation (caries, large restorations, marked mobility); and inability to follow written or auditory instructions. Cone-beam computed tomographic (CBCT) images were made and used to: estimate mandibular condylar rectilinear loading area based on axial plane dimensions: major axis X minor axis (mm-squared); measure mandibular plane angle (Frankfort horizontal to mandibular plane); ramal length (condylion to gonion); and mandibular length (maximum length of condyle to pogonion, mm); and construct three-dimensional anatomical geometry files of the positions of mandibular condyles, teeth, and positions and orientations of masseter, temporalis, medial and lateral pterygoid, and digastric muscles. Computer-assisted numerical models, with the objective of minimization of joint loads or muscle effort, were used with subject-specific geometry files to predict TMJ loads for a static-bite force of 10 N applied at a range of biting angles on the mandibular right first molar in the retruded and protruded mandibular positions and the central incisor in the protruded mandibular position. Estimated TMJ compressive stresses (N/mm-squared, MPa) were calculated using the predicted TMJ loads divided by the estimated condylar loading area for the ipsilateral (right) and contralateral (left) mandibular condyles in each subject. Two-sample and paired t-tests were used to evaluate differences in TMJ loads and estimated compressive stresses for molar and incisor biting in the retruded and protruded mandibular positions, where $p<0.05$ was considered statistically significant. Regression analyses were used to test for correlations of TMJ loads and of compressive stresses with sex, age, mandibular plane angle, ramal length, and/or mandibular length.

Results

Seven males and five females met inclusion criteria and did not meet exclusion criteria. Intraclass coefficients determined excellent intrarater reliability. TMJ loads and compressive stresses were significantly greater for incisor biting in the protruded mandibular position compared to molar biting in the protruded mandibular position (all p£0.002 and p<0.001, respectively). For pooled biting conditions and sexes, within condyle sides, there were no significant differences in TMJ compressive stresses between unilateral molar biting in the retruded and protruded mandibular positions (all p>0.18). There were no sex differences for TMJ compressive stresses for any of the biting or mandibular positions. Regression analyses of TMJ load (% of applied bite force) versus mandible length (mm), and Co-Go length (mm) showed positive correlations for both ipsilateral and contralateral TMJs for molar biting in the retruded mandibular position (R-squared = 0.69, R-squared = 0.46, respectively) and incisor biting in the protruded mandibular position (R-squared = 0.24, R-squared = 0.30, respectively). Regression analysis showed increased age and decreased ipsilateral TMJ compressive stress were non-linearly correlated with increased mandibular length (R-squared = 0.52).

Conclusions

In a pediatric population before orthodontic treatment: 1A. Predicted TMJ loads (% applied bite force) and 1B. TMJ compressive stresses (MPa) were significantly greater during unilateral incisor biting with the mandible protruded to class I occlusion compared to unilateral molar biting with the mandible in the retruded and protruded positions, but not different during unilateral molar biting with the mandible in protruded compared to retruded position: 2A. Both ipsilateral and contralateral TMJ loads for unilateral biting on molars with the mandible in retruded position and incisors with the mandible in protruded position were positively correlated with mandibular and ramal lengths; and 2B. Increased age and decreased ipsilateral TMJ compressive stress were non-linearly correlated with increased mandibular length. Thus, increased age in the range between 10-14 years and relatively lower ipsilateral TMJ compressive stresses may be possible pre-treatment clinical indicators of predicting success with mandibular orthopedic appliances.

Evaluating Patient Behavior Pre-operatively and Post-operatively Following Dental Treatment Under Moderate Sedation and General Anesthesia: A Retrospective Review

Jay Kim
Resident, Pediatric Dentistry, OHSU School of Dentistry

Co-Authors: Jacy Stauffer

Introduction
Pediatric dentists work as a team with young patients and their parents to not only restore dentition but also help set the patient up for future oral health success by creating positive dental experiences. Dentists use advanced pharmacologic behavior management for children to deliver safe and successful treatment after a thorough assessment of the child's behavior and medical conditions. Providers and parents have hope in eventually having child acceptance and cooperation for dental treatment after overcoming initial dental anxiety. Studies show improvement in quality of life and dental behavior at 6- and 12-month recall appointments following procedures completed under general anesthesia (GA). This study evaluates change in behavior in children that received dental treatment under moderate sedation (MS) or GA by comparing Frankl Behavior Rating Scale (FBRS) values recorded at pre-operative and subsequent post-operative visits.

Methods
This study did a retrospective chart review of patients in ages 1-12 years old who received MS or GA from 01/2019 to 01/2021 with follow-up visits in 6-months, 12-months, and/or 18-months.

Results
There was a positive change in behavior in patients who received dental treatment under GA except in patients with significant comorbidities (ASA III). There was no statistically significant difference in behavior in patients who received treatment under MS.

Conclusions
MS or GA may impact future behavior compliance but cannot be isolated as the sole cause of behavior improvement. Behavior change is a multifactorial result of the child's cognitive development, mood, time of day, provider, parental guidance, and memories of experience outside the dental clinic. Further research needs to be done on how GA and MS experience affects a child's psyche due to inconclusive data and subjective values of Frankl scores.

Rapid FTIR-ATR Spectroscopic Imaging for Analysis of the Dentin/adhesive Interface

Steven Lewis

Research Project Manager, Pfeifer lab, OHSU School of Dentistry

Co-Authors: Fernanda Tsuzuki, Carmem Pfeifer

Introduction
Hydrolytically-stable acrylamides can preserve the integrity of the bonded resin/dentin interface in 2-step, total etch adhesives (Fugolin et al., 2019). Recent advancements in Fourier transform infrared (FTIR) microscopy coupled with attenuated total reflectance (micro-ATR) have enabled rapid and precise chemical mapping alongside high-resolution visual surface imaging. This work evaluated the fidelity of FTIR-ATR microscopy as a tool for characterizing the adhesive and hybrid layer regions in dental restorations containing either traditional methacrylate-based or acrylamide-based adhesives.

Methods
Acidic primers were comprised of 45wt% N,N-Diethyl-1,3-bis(acrylamido)propane – DEBAAP or 2-hydroxyethyl methacrylate – HEMA, 10wt% 10-MDP (10-methacryloyloxydecyl dihydrogen phosphate) and 45wt% glycerol dimethacrylate – GDMA. Adhesives contained 45wt% DEBAAP or HEMA, 10 wt% 10-MDP and 45wt% urethane dimethacrylate (UDMA). Camphorquinone, ethyl-4dimethylaminobenzoate, diphenyliodonium hexafluorophosphate and butylhydroxytoluene were used as initiators and inhibitors (0.2/0.8/0.4/0.1wt%, respectively). 1 mm2 stick specimens were prepared using human dentin, commercial composite (Filtek Supreme) and 5 primer/bond combinations: CC (Clearfil Primer and Bond), HH (HEMA/HEMA), DD (DEBAAP/DEBAAP), HD (HEMA/DEBAAP) and DH (DEBAAP/HEMA). A Nicolet RaptIR FTIR microscope equipped with a MCT detector and germanium-tip ATR was used to collect 300x20µm specimen maps spanning the composite, adhesive/hybrid layer and dentin. Mid-IR spectral data was collected in absorbance (64 sample scans, 16cm-1 resolution) between 4000-400cm-1. Contour fill plots and 3D colormaps of wavenumber versus peak intensity were generated using Origin and were compared with confocal laser scanning microscopy (CLSM) cross-sectional images of similar interfacial regions.

Results
Spectral features corresponding to dentin, adhesive and resin composite were identified in all groups. Amide and phosphate regions associated with collagen were apparent in the dentin regions (amide 1 – 1647cm-1, amide 2 – 1553cm-1, PO43- – 1013cm-1), while the adhesive layer displayed increased absorbance in the carbonyl (1720cm-1) and C-O (1165cm-1) vibrational stretches, consistent with methacrylate/acrylamide monomers. The IR-mapped region of the adhesive layer varied in thickness among the groups, with the HH group displaying the thickest layer at approximately 90 µm, while the DH and HD groups had thicknesses of approximately 40 µm. By contrast, CLSM showed HH had the thinnest adhesive layer, but a greater depth of penetration into the dentin. Regions of overlap were more difficult to elucidate using FTIR-ATR microscopy.

Conclusions
FTIR-ATR microscopy is a powerful tool for rapid measurement and visualization of compositional differences in the resin-dentin bonded interface. Additional studies are underway to optimize the primer and adhesive formulations with the goal of maximizing bond strength through the addition of acrylamides.

Design and validation of a co-polymerizable MMP inhibitor

Matthew Logan
Instructor, Pfeifer lab, OHSU School of Dentistry

Co-Authors: Luke Miller, Fernanda Sandes De Lucena, and Carmem Pfeifer

Introduction
Matrix metalloproteinases (MMPs) have been shown to decrease the stability of the bonded interface through collagenolytic activity. A well-studied and potent hydroxamic acid MMP inhibitor, NNGH, was chosen as a scaffold for the design of a co-polymerizable restorative material capable of long-lasting inhibition of MMPs. This study works to design and validate hydroxamic acid derivatives to characterize the area protein leading out of the active site and to identify a candidate compound for functionalization with a linker and polymerizable moiety.

Methods
Hydroxamic acid derivatives of the parent inhibitor compound, NNGH, were designed and synthesized with terminal methoxy groups and linkers of varying length and polarity. A carboxylic acid version of NNGH was used to represent the hydrolysis of the zinc binding hydroxamic acid. Derivatives were modeled (Chimera/Autodock Vina) in active site of MMP2/9 and given a docking score. MMP activity was determined using a commercial kit (EnzChek Gelatinase/Collagenase Assay Kit; Molecular Probes). Data were fit to a non-linear curve (one phase decay) to determine IC50 values.

Results
The parent molecule, NNGH, had the best docking score, -6.5 kcal/mol, and most potent IC50, 0.16 ± 0.06 µM. The synthesized derivative were observed to have slightly lower docking scores and IC50 values compared to the parent NNGH compound. The carboxylic acid analog derivatives performed much worse than their hydroxamic acid counterparts in both docking score and IC50. Hydroxamic acids bind much tighter to zinc than carboxylic acids so this trend is expected. While the derivatives showed slight reduction in IC50, it was not as large of a decrease as the carboxylic acid analogs, indicating that the compound is binding with zinc and is oriented correctly in the active site with the methoxy "linker" pointing out of the enzyme.

Conclusions
Although less potent, the NNGH derivatives provides evidence that the NNGH scaffold has potential to be functionalized as a co-polymerizable restorative material. Incorporation of a polymer bound MMP inhibitor could result in long lasting inhibition of collagen degradation by MMPs. Future work will include synthesis that incorporates a PEG linker and methacrylate group onto the NNGH scaffold to allow for incorporation into dental adhesive formulations.

Nanomolar inhibitor of MMP activity for hybrid layer preservation

Fernanda Lucena
PostDoctoral Scholar, Pfeifer lab, OHSU School of Dentistry

Co-Authors: Matthew Logan, Jade Wong, Steven Lewis, Carmem Pfeifer

Introduction
N-Isobutyl-N-(4-methoxyphenylsulfonyl)-glycyl hydroxamic acid (NNGH) has been shown to strongly inhibit MMP3 and modulate cancer progression and metastasis. This study aims to evaluate its potential effect in preserving the hybrid layer, and increasing the longevity of dental restorations.

Methods
MMP-2 and -9 activity was measured through a fluorometric assay using DQ™-gelatin as substrate. Rat tendon collagen (RTT) degradation was measured in disks (n=3) crosslinked with NaOH/DMEM. Disks were incubated with collagenase solution with no inhibitor, 50µM or 100µM NNGH, at 37°C for 6, 24 or 72h. Lyophilized discs were weighed and imaged with SEM. Microtensile bond strength (MTBS) was assessed in human third molars restored with BisGMA/HEMA experimental adhesives with 0 or 50/100µM NNGH in a 40% EtOH solvent system, with or without dentin pre-treatment with 50µM NNGH solutions. 1x1 mm2 sticks were incubated in water or biofilm for 1 week (n=3). Data were analyzed with one-way ANOVA or Kruskal-Wallis/Tukey's test (α=0.05).

Results
Enzymatic activity of both MMPs -2 and -9 was significantly reduced with all NNGH concentrations (p<0.001). The collagen degradation statistically increased with incubation time (p<0.001) except for 100µM NNGH, where no degradation was observed compared to the control (p<0.001). The MTBS was not affected by the addition of NNGH (water: p=0.052; biofilm: p=0.175). However, the control groups showed statistically significant reduction in MTBS between water and biofilm storage, whereas the NNGH groups were able to sustain MTBS values after being challenged in biofilm.

Conclusions
NNGH was able to inhibit MMP activity at the nanomolar scale, which led to reduced collagen degradation at 100µM. The groups pretreated with NNGH solutions or restored with NNGH-containing adhesives were able to sustain MTBS values after tested in biofilm.

Salivary biofilm complex model to evaluate bacterial activity in dental materials.

Maria Eduarda Marinho
PhD Student, Pfeifer lab, OHSU School of Dentistry

Co-Authors: Fernanda M. Tsuzuki, Steven Lewis, Carmem S. Pfeifer

Introduction

In many analyzes of bacterial activity in dentistry, the inoculum is normally composed of a single species of bacteria: Streptococcus mutans. However, microcosms are laboratory models that mimic the conditions of the original environment. They are taken from that environment, maintaining complexity and heterogeneity. These models allow replicating bacterial community dynamics in the laboratory, facilitating the manipulation of variables of interest. Therefore, the aim of this study was to compare bacterial activity between a hydrophilic and a hydrophobic material in the presence or absence of acquired pellicle salivary using a microcosm biofilm model from an inoculum derived from saliva.

Methods

BisEMA and PEGDMA (hydrophobic and hydrophilic materials, respectively) were mixed with 0.1 wt% DMPA (photoinitiator). Discs (10 mm in diameter and 0.8 mm in thickness) were photoactivated (Acticure 4000 UV Cure, 630 mW/cm2, 320-500 nm), then sanded with #1000 sandpaper, to standardize the roughness value between 0.4-0.7 µm. Four groups were analyzed: PEGDMA and BisEMA with or without acquired pellicle (n=2). For acquired pellicle formation, the saliva supernatant obtained from 8 healthy donors (ages 20-45, both genders) was centrifuged for 10 min at 4°C (4000 rpm), then used to incubate the discs for 2 hours at room temperature (24±1 °C). After the formation of the acquired salivary pellicle, the samples were placed on sterile 24-well plates with 1.5 mL of a solution composed of McBain and saliva with glycerol (1/50 proportion). The samples were kept for 48h in contact with McBain for biofilm formation at 37 °C and 5% of CO_2. Biofilm formation on the surfaces was evaluated by counting colony forming units (CFU/mL) and then the numbers were tallied and converted to log_{10} CFU/mL. Data was analyzed with one-way ANOVA/Tukey's test (alpha = 5%).

Results

For CFU counting, brain-heart infusion agar (BHI) was used to evaluate total microorganisms, mitis salivarius agar (MSA) evaluated the total Streptococcus spp, modified mitis salivarius agar with 20% sucrose (SB-20) was employed to evaluate Streptococcus mutans, and Rogosa agar (MRS) was utilized to evaluate Lactobacillus spp (n=4). Preliminary results showed that there was no statistical difference in total microorganisms (BHI) (p=0.364). For Lactobacillus (MRS), BisEMA in saliva exhibited the highest growth ($1.48 \times 10^3 \pm 2.81 \times 10^2$) CFU/mL (p<0.001). This finding was similar for Streptococcus mutans (SB-20), where BisEMA was statistically different from all other groups ($1.2 \times 10^3 \pm 2.07 \times 10^2$) CFU/mL (p=0.004). For MSA, the lowest growth of Streptococcus spp was found for PEGDMA in water ($6 \times 10^2 \pm 1.93 \times 10^2$) CFU/mL (p=0.030).

Conclusions

BisEMA exhibited a higher quantity of Streptococcus and Streptococcus mutans. In samples containing saliva instead of water, there was a greater growth of total microorganisms, Lactobacillus, Streptococcus, and Streptococcus mutans. All media had growth of a single type of bacteria, except BHI, where different colonies were observed. These findings suggest that the characteristics of the culture medium and the material can influence bacterial growth. It is concluded that this biofilm model can be used to evaluate bacterial activity on dental materials.

Investigating diadenylate cyclase (DAC) and protein-protein interactions in Streptococcus mutans

Rong Mu
Senior Research Associate, Wu lab, OHSU School of Dentistry

Co-Authors: Hua Zhang, Hua Qin, Justin Merritt and Hui Wu

Introduction

Diadenylate cyclase (DAC) plays an important role in catalyzing the synthesis of a singular c-di-AMP molecule from either two ATP or ADP molecules. This essential secondary messenger, c-di-AMP, has been identified in Gram-positive bacteria, Gram-negative bacteria, and certain Archaea, participating in cell signaling, influencing and regulating essential cellular processes. Building upon known interactions with GlmM and CdaR proteins, regulators of c-di-AMP levels, our study seeks to expand this knowledge by identifying novel proteins influencing DAC through protein-protein interactions, which will shed light on DAC's diverse cellular roles and uncovering potential regulatory mechanisms.

Methods

We used Streptoccocus mutans as our study model. To uncover potential protein interactions with DAC, we employed co-immunoprecipation followed by mass spectrometry. In brief, we introduced a FLAG tag to the C-terminal of DAC and purified the resulting FLAG-tagged DAC from both crosslinked and non-crosslinked cell lysates using an anti-FLAG resin column. The masses of the purified proteins were then analyzed through mass spectrometry. To validate the protein-protein interactions identified by mass spectrometry in vivo, we utilized an intermolecular split luciferase assay. In this assay, two domains of luciferase were attached to each partner of two interacting proteins. Upon interaction, luciferase fragments were brought close together, forming a complemented luciferase that produced a luminescent signal upon the addition of substrates. Additionally, we employed the API20 strep kit to investigate metabolism correlations between DAC and its potential interacting proteins. This involved generating gene knockout mutants and cultivating the bacteria in THB medium within a CO_2 incubator until reaching an OD600 of 0.8.

Results

Our mass spectrometry proteomic screen has broadened the list of potential interacting proteins with DAC, in addition to the previously reported GlmM and CdaR proteins. Several selected proteins from the mass spectrometry data were reconfirmed for their interaction with DAC in a cellular environment through the intermolecular split luciferase assay, thereby enhancing the relevance of our mass spectrometry data in terms of involvement in DAC interactions. Additionally, we have chosen specific proteins from the mass spectrometry data for further investigation through mutagenesis and metabolism studies. Notably, the absence of proteins such as SMU_1200 and SMU_723 results in a defect in sorbitol metabolism similar to that observed in the DAC mutant, suggesting their potential interaction with DAC could impact this metabolic pathway.

Conclusions

Our mass spectrometry proteomic screen robustly affirms the previously documented interactions between DAC and both GlmM and CdaR proteins. Through the intermolecular split luciferase assay, several candidate proteins identified in our mass spectrometry data were successfully reconfirmed for their interactions with DAC in a cellular environment. The

identification of established protein interactions and the reaffirmation of in vivo protein-protein interactions through our mass spectrometry data solidify a foundation for exploring further interactions involving the DAC protein. Furthermore, the combination of gene mutagenesis with the API20 strep assay enabled the identification of proteins implicated in the same metabolic pathway as the DAC mutant, which implies that the interactions with DAC could play a contributory role in this shared pathway.

Anaerobic Protein Expression in Benign vs. Malignant Head and Neck Tumors: a Pilot Study

Jonathan Nguyen
DMD Student, OHSU School of Dentistry

Co-Authors: Farah Karim1, DDS, MS, Srinivasa Chandra2, MD, BDS, FDSRCS, FIBCOMS,

1University of Washington School of Dentistry, Seattle WA.

2Oregon Health and Science University School of Dentistry, Portland OR. 2Oregon Health and Science University School of Dentistry, Department of Oral and Maxillofacial Surgery, Portland, OR

Introduction

Increased expression of three proteins related to glycolytic metabolism, glucose transporter 1, lactate dehydrogenase A, and monocarboxylate transporter 4, is associated with oral squamous cell carcinoma (OSCC) metastasis and recurrence. Ameloblastomas, odontogenic myxomas, and keratocystic odontogenic tumors are clinically aggressive, benign odontogenic neoplasms that frequently invade adjacent tissues and demonstrate high postoperative recurrence rates despite marginal resectioning. These observations suggest growth mechanisms in benign tumors that resemble those of malignant tumors. It is hypothesized that benign odontogenic tumors undergo a shift in metabolic activity as is seen in malignant cancers, and consequently express certain anaerobic proteins at levels similar to OSCC.

Methods

Cross-sectional study to assess the expression of GLUT1, LDHA, and MCT4 in biopsy specimens of benign odontogenic tumors. Specimens were prepared by formalin fixation in 10% neutral buffered formalin, embedded in paraffin, and cut into 3-5 micron sections. Samples were obtained from the NWBioSpecimen and antibodies from Santa Cruz Biotechnology. Inclusion criteria: All tumor samples were resected between 2014-2015 and had grown over 2 cm in vivo. Exclusion criteria: Specimens subjected to neoadjuvant therapy. Predictor variables: Tumor type: 1) ameloblastoma (n=1), 2) OM (n=1), 3) KCOT (n=1), and 4) OSCC (n=1). Outcome variables: Nuclear and cytoplasmic IHC staining intensity levels of GLUT1, LDHA, and MCT4 in each tumor sample. Staining intensity was scored as strong (3), moderate (2), mild (1), or absent (0) staining.

Results

Ameloblastoma and KCOT cells express GLUT1 and LDHA at intensity levels similar to OSCC cells. OM cells express LDHA at intensity levels similar to OSCC, but do not express GLUT1. Analysis of the MCT4 stain showed absent (0) staining in the ameloblastoma, KCOT, OM, and OSCC samples. This is inconsistent with previous studies on MCT4 and OSCC. Further research needs to be done to examine MCT4 expression in benign odontogenic tumors.

Conclusions

This study presents novel findings on the expression of GLUT1 and LDHA in ameloblastoma, KCOT, and OM neoplasms, and raises the possibility that these glycolytic proteins could serve as potential targets in the development of gene-targeted odontogenic tumor therapy in the future. Future studies will include a larger sample size and focus on using qPCR and DNA microarray analysis to quantify anaerobic protein expression in odontogenic tumors.

Self-Sterilizing Surfaces Using Quaternary Ammonium Methacrylates and its Zwitterion

Peter Nguyen

DMD Student, OHSU School of Dentistry

Introduction

Direct restorations using a self-sterilizing resin composite that prevents the formation of secondary caries would have increased longevity. Carboxybetaine methacrylate (CB-MA) is a monomer that switches between an antimicrobial cationic ring (QAM) and its antifouling linear zwitterion (ZWIT). Previous research in the Pfeifer Lab has shown that increased CB-MA substituents can upshift pH at which the QAM-ZWIT switch occurs at. The goal of this project was to decouple the role of charge concentration and side chain length on the antimicrobial effect of model QAM-ZWIT molecules.

Methods

A static CB-MA equilibrium was created with resin composite discs of six percent mass weight QAM and ZWIT at different mol ratios (0:100, 20:80, 40:60, 60:40, 80:20, 100:0; n = 6). Degree of conversion was assessed with FT-IR. Hydrophilic character of the surface was measured with contact angle experiments. S. mutans biofilm was grown on the discs for 6 hours in a 5% CO_2 incubator. Supernatant bacteria levels were measured using planktonic optical density before being used to test bacteria viability with colony forming units. Disc-surface biofilm was measured using biofilm optical density, and a luciferase assay was used to measure metabolism. Finally, a crystal violet assay was used to quantify biomass. Data were analyzed with one-way ANOVA/Tukey's test (alpha=5%).

Results

The addition of QAM and ZWIT did not significantly affect the degree of conversion or the contact angle. There was no significant difference in supernatant bacteria levels, but the bacterial viability significantly decreased as QAM increased. The bacteria on the discs showed no difference in metabolism even though there was significantly less biomass.

Conclusion

The results provide a starting point to determining the minimum percentage by mass weight of QAM required for an antimicrobial resin composite surface. A fluorescein assay combined with UV-vis spectroscopy will be used to measure how much of the QAM is on the surface of each resin composite disc. An impingement test will be used to measure biofilm removed by water to correlate it to attachment strength. Ultimately, the goal of this investigation is to design smart, pH-sensitive switching materials to maximize anti-biofilm potential in restorative applications.

Autonomic Function and Muscle Activity in Growing Children

Jeff Nickel

Professor, Division of Orthodontics and Dentofacial Orthopedics, OHSU School of Dentistry

Co-Authors: Myriam Hamieh, Laura Iwasaki, Elizabeth Palmer, Dongseok Choi

Introduction

The study sought to examine the relationships between ramal height, autonomic nervous system activity, as measured by the heart rate variance in inter-beat intervals, and masticatory muscle activity gauged by duty factors in circumpubertal children aged 10-14 years at the CVM3 stage. While age, masseter and temporalis muscle duty factors, and ANS tone (pNN50 and LF/HF) served as independent variables, ramus height was treated as the dependent variable. Our null hypothesis posited that there was no significant correlation between ramal height (mm), nocturnal autonomic nervous system activity (LF/HF; pNN50) and nocturnal masticatory muscle activity (Duty Factor, %) in circumpubertal children.

Methods

According to OHSU IRB oversight, skeletal Class II children participated. CBCT images were used to measure mandibular ramus height. Laboratory protocols quantified masticatory muscle activity per N of biting force. Subjects were trained how to use a portable EMG/ECG recorder. Over four nights, the recorder captured masticatory and heart muscle activities. The nocturnal activity of the autonomic nervous system (ANS) was characterized by analyses of heart rate variability (HRV) using commercial software (MindWare™). Specifically, night-time ultradian cycling of sympathovagal balance, and parasympathetic activity, were estimated per 5 minute windows. Nocturnal ultradian cycling sympathovagal balance was characterized by a high order polynomial. At each peak and valley of the polynomial, masseter and temporalis muscle EMG data corresponding to loads between >1 and <5 Newtons, and HRV data were calculated. 2D and 3D non-linear regression analyses were used to test for correlation between dependent variable of ramus height (Co-Go), and the independent variables of muscle activity/ANS regression slopes, and age (years).

Results

Fifteen participants enrolled (nine males and six females), with an overall average age of 13.1 ± 1.3 years. Two subjects were unable to provide complete recordings. Analysis of sympathovagal tone (LF/HF ratio) and pure parasympathetic activity (pNN50) across peak-valley 20-minute epochs revealed consistent patterns. Masseter muscle activities per ANS activities (muscle duty factors vs. LF/HF, and pNN50), regression slopes and y-intercepts varied, with R^2 values indicating varying degrees of correlation (average R^2 for LF/HF:+ 0.66 ± 0.22; average R^2 for pNN50: -0.42 ± 0.21). Reliability tests for mandibular ramus height measurements (Co-Go) displayed high Pearson's Correlation and Intraclass Correlation Coefficient values (0.99). The 3D regression analysis demonstrated that approximately 52% of the variance in dependent variable of ramus height could be explained by the combined effects of the independent variables of age and masseter muscle duty factor per LF/HF activity.

Conclusions

In this study, our results demonstrated correlations between mandibular ramal height, increased nocturnal sympathovagal tone, and increased nocturnal masseter muscle activities between 1 and 5 newtons, in circumpubertal children with Class II malocclusions.

The Impact of the American Dental Association Antibiotic Prescribing Guidelines on prescribing practices within a Dental School Setting

Ahmad Oubaid
Resident, Endodontics, OHSU School of Dentistry

Co-Authors: Replogle, Karan; Dongseok, Choi

Introduction
The American Dental Association (ADA) published a report in 2019 providing evidence-based clinical practice guidelines for the urgent management of pulpal and periapical related dental pain and swelling. The purpose of this retrospective study is to evaluate the prescribing practices before and after ADA guidelines for patients who received evaluation and/or treatment at the Graduate Endodontic Clinic (GEC) at Oregon Health & Science University School of Dentistry. The congruence of prescribing practices to the guidelines and factors associated with lack of congruence was investigated.

Methods
Electronic health records (axiUm®) from all patients evaluated and/or treated in the GEC from 2016 to 2023 were reviewed retrospectively. Data was retrieved for the period from September 2016 through November 2019 as the "time before ADA evidence-based guidelines". Data from November 2019 through January 2023 was retrieved as the "time after ADA evidence-based guidelines". Each period covered 1,156 days (38 months) on either side of the date of implementation of the ADA Guidelines.
Data pulled included, antibiotic prescribed, date of prescription and common dental terminology (CDT) code. Additional data was extracted regarding patient age, gender, pulpal and periapical diagnosis, pain level, presence and absence of signs and symptoms of systemic involvement. To compare the prescribing practice before and after the guidelines, prescribing rates were calculated and analyzed. The data was analyzed using descriptive statistics and chi-square tests of independence. Significance was set at $P<0.05$.

Results
to be determined

Conclusions
to be determined

Antimicrobial oligomeric additives for dental adhesives and composites

Clara Park
DMD Student, OHSU School of Dentistry

Co-Authors: Sarah Patty, Fernanda Sandes De Lucena, Steven Lewis, Carmem Silvia Pfeifer
Oregon Health & Science University, Biomaterial and Biomedical Sciences

Objective

Composite restorations have been shown to be compromised by secondary caries formation. One quaternary ammonium-containing monomer (QAT), dimethylaminohexadecyl methacrylate (DMAHDM) has shown antimicrobial properties, but at high concentrations, may compromise mechanical properties. The aim of this study is to overcome this issue by tethering QATs to a thiourethane-based oligomer, known to increase toughness in composites.

Methods

One thiourethane oligomer was synthesized as previously described. The pendant thiol content was determined with iodometric titration. DMAHDM was reacted in a 0.1 mol equivalence of SH, confirmed through NMR/IR spectroscopy. 5wt% of DMAHDM:TU was solubilized BisEMA:UDMA:TEGDMA (50:30:20 wt%, BUT), made polymerizable with camphorquinone/amine. Resin discs were photoactivated at 109 mW/cm^2 for 2 minutes each side, then roughness and polymerization conversion (by near-IR) were determined. *S. mutans* biofilm viability (luciferase assay) and biomass (crystal violet assay) were assessed. Data were analyzed with one-way ANOVA/Tukey's test (alpha=5%).

Results

Data for biofilm viability and biomass are shown in the Table (arbitrary units; same superscript indicates statistical similarity). At the QAT concentration used for the TU:DMAHDM synthesis, the oligomer was not easily dissolved in the resin matrix. BUT:TU:DMAHDM led to no reduction in the biofilm viability (p=0.0728) or biomass (p=0.2803) compared to the controls for both planktonic and biofilm-bound bacteria.

	Luminescence x10^6 (viability) - planktonic	Luminescence x10^6 (viability) - biofilm	Absorbance (biomass)
BUT	1.2±1.6[a]	8.7±3.4[a]	2.35±0.60[a]
BUT:TU	1.5±0.5[a]	6.0±2.4[a]	2.36±0.42[a]
BUT:TU:DMAHDM	0.9±0.8[a]	6.0±2.3[a]	2.85±0.39[a]

Conclusions

The high QAT concentration on the TU oligomer impaired solubility in the resin matrix. The resulting increased roughness of the surface masked any potential differences in antimicrobial effect. Future studies will include synthesis of TU oligomers with lower QAT content, which should improve its dispersion in the resin matrix and allow for higher concentration of QAT in the material overall.

Central Venous Catheter Modifications with Covalently Anchored Antimicrobials & Antithrombogenics for Biofilm Inhibition: proposed project

Sarah Patty
Research Associate, Pfeifer lab, OHSU School of Dentistry

Co-Authors: SH Lewis, S. Weber, CS Pfeifer

Introduction
Prior research incorporating quaternary ammonium-based molecules (QA) onto restored dental surfaces showed promising reduction in biofilm colonization. Leveraging similar QA technology onto the surface of medical devices could greatly reduce other types of infection, particularly healthcare-associated infections (HAIs). Central venous catheter (CVC) devices are considered the primary source of hospital-acquired bloodstream infection. Approximately 5 million CVCs are inserted per year, and of these, 3-8% of placed CVCs lead to infection, which increases morbidity and retreatment costs for patients. The purpose of this investigation was to characterize commercially available CVCs, and generate synthetic strategies to improve their success.

Methods
Five different polyurethane catheters were obtained, 3 of which were coated with antimicrobial or antithrombogenic compounds, with the chemical structure remaining unspecified by the manufacturer. CVCs were obtained from Cook, Teleflex, and Angiodynamics and were analyzed with no chemical modification by infra-red spectroscopy. Reference polyol and polyurethane materials were used for comparison. Catheter tubing was analyzed by making vertical, horizontal, and angled cross-sectional cuts into the tubing. Spectra were collected under ambient conditions (4000-400 cm-1). Qualitative visual assessment as well as OMNIC software library searches against reference components were used to make conclusions about approximate chemical structure. The next phase of the study will involve synthesis of polyurethanes functionalized with QA, antimicrobials known to prevent central line-associated bloodstream infection (such as taurolidine), and pH tunable antifouling/ antimicrobial molecules, such as carboxybetaines. These functionalized catheter materials will then be characterized by infrared spectroscopy to assess functionalization, crystal violet assay to assess biofilm inhibition and potential leachate analysis. Materials that demonstrate biofilm inhibition will then be further characterized for mechanical properties.

Results
Preliminary analysis of the infra-red spectra show expected carbonyl (C=O) peaks in both the 1750-1700 cm-1 and 1695-1690 cm-1 range for both the Teleflex coated and uncoated polyurethane catheters, consistent with the presence of both polyester- and polyurethane-associated C=O groups, respectively. This and the CNH group near 1540-1530 cm-1 are consistent with the general polyurethane composition disclosed by the manufacturer. The coated polyurethane catheter from the same manufacturer has a relatively higher polyurethane-associated C=O peak compared to the polyester C=O peak, and in addition, has a much broader NH region. This could be due to higher NH contribution and hydrogen bonding from chlorohexidine coating. While we cannot identify the antimicrobial compounds reportedly coated onto the Cook antimicrobial catheter surface, we expect significant differences in the spectra

between coated and uncoated materials, mostly in the C=O and NH regions, indicating potential presence of more hard segments and high hydrogen bonding potential.

Conclusions
The materials analyzed so far are consistent with disclosed compositions, which will inform the design of novel materials modified with QA. Materials marketed as "antimicrobial" show higher NH regions, suggesting increased hydrophilicity is a significant contributor for biofilm inhibition and antithrombogenicity in CVCs.

The Effect of Social Stories on Children's Behavior in a Pediatric Dental Clinic: A Pilot Study

Edward Pham
Resident, Pediatric Dentistry, OHSU School of Dentistry

Co-Authors: Jacy Stauffer, DMD

Introduction

The objective of this study was to evaluate the effect of video social stories on behavior for new patients in the Oregon Health & Science University (OHSU) Pediatric Dental Clinic.

Methods

A retrospective chart review in Axium electronic health record was conducted from 2020-2023 to establish the control group (Group 1). The intervention (Group 2) comprised of a video social story which was recorded at the OHSU Pediatric Dental Clinic. Group 2 subjects were contacted by phone and received via e-mail the pre- and post-intervention surveys, and social story video. Participants were eligible to participate if they had an upcoming new patient exam and had no previous encounter on file. Participants were asked about demographics, parental perceptions of their own and child's level of anxiety and fearfulness, as well as expected behavior of the child. Surveys consisted of multiple-choice, Likert scale, and open-ended questions. Behavior was measured using the Frankl Score. Data analysis utilized BlueSkyStatistics v. 10.2.1.

Results

The retrospective chart review yielded 1717 records, and a total of 73 were included in the Group 1. Thirty-seven subjects (Group 2) were reached by phone and received the pre-intervention survey and video. A response rate to the pre-intervention survey was 22/37 (59%). Due to loss of subject enrollment, the response rate to the post-intervention survey was 7/22 (32%). Average Frankl score for the control group was 3.13 and the intervention group was 3.09. ***Further results pending return of post-intervention survey***

Conclusions

Pending final data analysis with post-intervention survey

Vascularized Bone-like Organoids: A Model System And Regenerative Strategy

Genevieve Romanowicz

PostDoctoral Scholar (T90 PORT Trainee), Guldberg lab, Knight Campus for Accelerating Scientific Impact, University of Oregon

Co-Authors: Maggie Trail1, Ethan Dinh1, Kelly Leguineche1,
Samuel Lester1, Ella Leeson1, Angela Lin1,
Luiz E. Bertassoni2, Robert E. Guldberg1
1 Knight Campus for Accelerating Scientific Impact, University of Oregon, Eugene, OR, USA
2 Cancer Early Detection Advanced Research Center (CEDAR), Knight Cancer Institute, Oregon Health and Science University (OHSU), Portland, OR, USA

Introduction

Autologous bone grafts are the gold standard for osseous injury healing, offering dense mineralization, osteoinductive and angiogenic cues. Vascularized autografts are effective but limited in size and require additional surgery. Recent tissue engineering advances replicate native bone characteristics without growth factors, allowing modular encapsulation of bone marrow stromal cells and endothelial cells. We developed vascularized bone-like organoids as an autograft alternative. We hypothesized that vascularity would enhance mineralization and mature bone phenotypes in our organoid model. Robotic bioprinting enabled scalable production of these organoids, presenting a novel approach to study the interplay between vascular and bone marrow stem cells in-vitro.

Methods

Organoid Fabrication: Cell-laden mineralized collagen was prepared as described1, briefly, rat tail type I collagen (3 mg/mL, Gibco) and human BMSCs (Lonza) were mixed to a final concentration of 1.5 mg/mL collagen containing either BMSCs (3.9x105 cells/mL) or BMSCs plus rat adipose derived microvascular fragments2 (MVFs) (20,000 fragments/mL). The hydrogels were cold (4ºC) printed in 2 µL using the BioAssembly Bot® 400 robotic bio-printer, then assembled into large volume flasks and agitated over the period of mineralization using described methods1, followed by standard culture conditions up to 12 days.
Histology: The resulting cellular organoids were decalcified then processed for hematoxylin and eosin staining.
Mineral Characterization: Standard and ultra-high resolution microcomputed tomography (microCT) as well as Fourier transform infrared spectroscopy (FTIR) were performed on mineralized and non-mineralized samples for each group of BMSCs only or BMSCs+MVFs (n=3-5 organoids/assay/group)(Unpaired, two tailed t-tests were used when comparing two groups, otherwise a one-way analysis of variance (ANOVA) was applied). Significance defined as a p-value < 0.05.

Results

The mineral to matrix ratio was 34% higher in the MVF+MSC bone-like organoids (3.56±0.32) as compared to MSC alone (2.33±0.30) (p=0.002) (Fig. 1A). The hydroxyapatite carbonation was higher in the MVF+MSC bone-like organoids (0.127±0.003) as compared to MSC alone (0.118±0.005) (p=0.05) (Fig. 1B), but no change in crystallinity (p=0.7). Microcomputed tomography (microCT) showed no difference in the bulk, average mineral density with or without MVFs. The mean densities were comparable with 283±109 mgHA/cm3 for MSC and 290±117 mgHA/cm3 for MSC+MVF. The higher density perimeter reached 430±64 mgHA/cm3 and

436±69 mgHA/cm3 for MSC and MSC+MVF, respectively. Histological sections revealed complex networks of pores which subsequently filled with either osteocyte-like cells (with mineral) or vasculature (without mineral) as the MVFs developed (Fig. 1C). Qualitatively, high resolution microCT showed increased mineral around encapsulated cells with MVFs as compared to BMSCs alone.

Conclusions

This study pioneers high-throughput robotic bioprinting to create cellularized, mineralized, and vascularized bone-like organoids with comparable mineral density to native bone. Microvascular fragment inclusion altered mineral/matrix ratios and carbonation, but not overall mineral density. Qualitative differences included enhanced pore formation and osteocyte-like cells in mineralized groups with microvascular fragment inclusion. These observations offer a unique opportunity to study bone differentiation and mineralization in under 12 days in-vitro, a departure from standard osteoblast/osteocyte differentiation studies. With further development, these organoids could serve as both a model for osteogenesis, a vascularized autograft alternative, and reduce the reliance on donor bone in surgery.

Fusobacterium nucleatum drives tumor-associated macrophage-like cells in an engineered oral squamous cell carcinoma on-a-chip

Mauricio Sousa

PostDoctoral Scholar (R90 PORT Trainee), Bertassoni lab, OHSU School of Dentistry

Co-Authors: Avathamsa Athirasala, May Anny Fraga, Dustin Higashi, Justin Merritt, Luiz Bertassoni.

Introduction
Oral squamous cell carcinoma (OSCC) is the sixth most prevalent cancer, representing 90% of all head and neck cancers. Oral cancers are expected to cause 11000 deaths in the US in 2023. OSCC comprises a complex microenvironment involving a 3D collagenous matrix, innate and adaptative immune cells, fibroblasts, and opportunistic microorganisms. Fusobacterium nucleatum, for instance, is related to OSCC development in different aspects, such as inducing epithelial-to-mesenchymal transition and coordinating the immunological response in the tumor microenvironment (TME). Although some advances were achieved in understanding the OSCC TME, there is an urge to develop advanced in vitro models to investigate the immunosuppressive role of opportunistic microorganisms in OSCCs. Offering a promising avenue for studying OSCCs, organs-on-a-chip serve as microphysiological platforms that closely emulate the complexities of biological tissues within the highly controllable microfluidic, cellular communication, and extracellular matrix.

Methods
Here, we developed an OSCC on-a-chip to understand the immunomodulatory profile of F. nucleatum on macrophages in the TME. We cultivated oral squamous carcinoma cells in 3D in a collagen matrix (2.5 mg/mL) in a microfluidic device that has a central chamber (1mm in width) and two lateral channels connected by triangular pillars (space between pillars of 115 µm). Our tested groups were collagen matrix containing OSCC (5.105 cells/mL) in the presence or absence of heat-killed antigens (1.106 CFUs/mL) from F. nucleatum (ATCC 23726). F. nucleatum cells were integrated with collagen gels and oral squamous carcinoma cells for three days. On the fourth day, we added 2.103 THP-1 derived macrophages (differentiated with PMA 100 ng/mL) in the lateral channel to evaluate their chemoattraction to the 3D matrix in the presence or absence of F. nucleatum for 48 hours.

Results
We noticed a significantly higher number of macrophages invading the 3D matrices that had heat-killed antigens when compared to the groups containing just OSSCs. By immunofluorescence, we stained the cells with markers for M1 (CD86) and M2 (CD163) and observed a significantly lower number of CD86 and a higher number of CD163-positive cells in the F. nucleatum stimulated group. When cytokines and chemokines were measured from these chips by Luminex assay, we found that the presence of heat-killed bacteria upregulated TNF-α, MCP-1, IL-6, VEGF, and CCL5 significantly, showing that the presence of F. nucleatum might stimulate tumor-associated macrophages-like cells.

Conclusions
These results enable us to understand how the early interactions between opportunistic microorganisms and the immune system modulate the suppression responses in the tumor microenvironment.

Mechanistic study of the antibiofilm effect of QAM-based materials

Jade Wong
Research Assistant, Pfeifer lab, OHSU School of Dentistry

Co-Authors: Fernanda Lucena, Matt Logan, Steven Lewis, Carmem Pfeifer

Introduction
The theory that, in positively charged molecules, longer side chains act as a lancet leading to bacterial disruption remains unproved. Given the flexibility and size of the chain compared with the thickness of the bacterial cell wall, the aim of this study was to elucidate the mechanism through which the combination of chain-length and charge in QAM-containing materials affects biofilm inhibition.

Methods
BisGMA/TEGDMA (50/50wt%), 0.1wt% DMPA, 70wt% filler were combined with 0 (control) or 10wt%: quaternary-ammonium methacrylate (QAM, positive charge) with 6- or 16-carbon side chain length (Q6 or Q16), or a zwitterion molecule (Z16, neutral) at several mol ratios (Figure 1A). Discs were photocured (700 mWcm2, 1 min/side), stored for 24 h, and the degree of conversion (DC) was measured (near-IR). Discs were sanded to 0.2-0.5μm surface roughness, then incubated with S. mutans (1% sucrose, TH media, 24 h, 37°C/5%CO2). Optical density of planktonic bacteria (OD), biofilm viability and biomass were assessed with crystal violet and luciferase assays. Data were analyzed with one-way ANOVA/Tukey's test (α=0.05).

Results
DC was statistically similar for all groups (p=0.117). Groups containing the long chain (Q16) presented overall lower values of OD (p<0.001), suggesting that potential leachates were affecting planktonic bacteria. In general, biofilm biomass and viability decreased with the increase of Q16 concentration. One interesting observation is that the combination Q16/Q6 led to statistically similar biofilm disruption than Q16/Z16 at the 60/40, and both were statistically similar to Q16 alone. Considering that Q6 alone has no antimicrobial effect, that indicates that charge concentration is the main driver of antibiofilm activity.

Conclusions
The results demonstrate that the side chain length is not the main factor in biofilm disruption with positively-charged molecules, since at the same charge concentration, a mixture of long and short-chains led to the same antibiofilm effect than the long-chain alone.